© 2021. Published by The Company of Biologists Ltd | Development (2021) 148, dev188755. doi:10.1242/dev.188755

RESEARCH ARTICLE

Itpr1 regulates the formation of anterior eye segment tissues derived from neural crest cells

Akira Kinoshita[1,*], Kaname Ohyama[2], Susumu Tanimura[3], Katsuya Matsuda[4], Tatsuya Kishino[5], Yutaka Negishi[6], Naoko Asahina[7], Hideaki Shiraishi[7], Kana Hosoki[8], Kiyotaka Tomiwa[9], Naoko Ishihara[10], Hiroyuki Mishima[1], Ryoichi Mori[11], Masahiro Nakashima[4], Shinji Saitoh[6] and Koh-ichiro Yoshiura[1]

ABSTRACT

Mutations in *ITPR1* cause ataxia and aniridia in individuals with Gillespie syndrome (GLSP). However, the pathogenic mechanisms underlying aniridia remain unclear. We identified a *de novo* GLSP mutation hotspot in the 3′-region of *ITPR1* in five individuals with GLSP. Furthermore, RNA-sequencing and immunoblotting revealed an eye-specific transcript of *Itpr1*, encoding a 218amino acid isoform. This isoform is localized not only in the endoplasmic reticulum, but also in the nuclear and cytoplasmic membranes. Ocular-specific transcription was repressed by SOX9 and induced by MAF in the anterior eye segment (AES) tissues. Mice lacking seven base pairs of the last *Itpr1* exon exhibited ataxia and aniridia, in which the iris lymphatic vessels, sphincter and dilator muscles, corneal endothelium and stroma were disrupted, but the neural crest cells persisted after completion of AES formation. Our analyses revealed that the 218-amino acid isoform regulated the directionality of actin fibers and the intensity of focal adhesion. The isoform might control the nuclear entry of transcriptional regulators, such as YAP. It is also possible that ITPR1 regulates both AES differentiation and muscle contraction in the iris.

KEY WORDS: Inositol 1,4,5-triphosphate receptor 1 gene (*ITPR1*), Anterior eye segment, Gillespie syndrome, Aniridia, Neural crest cell

INTRODUCTION

The vertebrate eye is a complex organ composed of many tissues; therefore, it exhibits a complicated developmental process. Interactions between the epidermal ectoderm and a neural-derived structure, originally called the optic vesicle but later known as the optic cup, result in the development of the lens, corneal epithelium and retina [reviewed by Adler and Canto-Soler (2007) and Heavner and Pevny (2012)]. Microtissues, such as the dilator and sphincter muscles of the iris, also develop from the optic cup ectoderm (Mann, 1925; Ferrari and Koch, 1984). The periocular mesenchyme, including neural crest cells (NCCs) and mesoderm cells, also participates in eye formation [reviewed by Cvekl and Tamm, 2004; Davis-Silberman and Ashery-Padan, 2008; Johnston et al., 1979; Trainor and Tam, 1995). In the mouse anterior eye segment (AES), the stroma and endothelium of the cornea, stroma of the iris and ciliary body, and Schlemm's canal wall originate from NCCs (Kanakubo et al., 2006). However, theories regarding the origin of AES remain controversial (Gage et al., 2005).

Aniridia (MIM: 106210) is a rare congenital eye anomaly that occurs in one in every 64,000-96,000 newborns (Shaw et al., 1960) and is defined as the complete or partial hypoplasia of the iris [reviewed by Jafari and Amiri (2015)]. Haploinsufficiency of the paired box gene 6 (*PAX6*, MIM: 607108), a master regulator of eye development, has been identified in individuals with congenital aniridia (Axton et al., 1997). However, several other transcription factors (TFs) contribute to eye development. For example, the v-MAF avian musculoaponeurotic fibrosarcoma oncogene homolog or MAF (MIM: 177075) is an important regulator of eye development, specifically that of the lens [reviewed by Eychène et al. (2008) and Xie and Cvekl (2011)]. In humans, heterozygous mutations in *MAF* cause ocular malformations, such as iris coloboma, congenital cataract, glaucoma, microcornea and microphthalmia (Anand et al., 2018). Furthermore, mutations in the genes encoding cytoskeletal proteins also cause iris malformations. Mutations in the actin genes *ACTB* (MIM: 102630) and *ACTG1* (MIM: 102560) cause iris coloboma in 70% of patients with Baraitser–Winter syndrome (Rivière et al., 2012). Mice with mutations in the unconventional myosin member *Myo6* (*tvrm89*), in which leucine at position 480 is replaced by proline, have been reported to exhibit iris malformation (Samuels et al., 2013). However, the detailed mechanisms by which these various genes cause iris malformations remain unknown.

Gillespie syndrome (GLSP, MIM: 206700) is a rare genetic disorder characterized by cerebellar ataxia, mild-to-severe intellectual disability and aniridia (Gillespie, 1965). Recently, five independent groups reported that the gene encoding inositol 1,4,5-triphosphate receptor 1 (*ITPR1*), located on 3p26.1, is mutated in GLSP (Gerber et al., 2016; McEntagart et al., 2016; Dentici et al., 2017; Carvalho et al., 2018; Paganini et al., 2018). ITPR1, a receptor for inositol 1,4,5-triphosphate (IP_3), functions as a calcium channel that mediates Ca^{2+} release from the endoplasmic reticulum (ER) upon stimulation by IP_3 (Maeda et al., 1990). Correspondingly, mutations or deletions of *ITPR1* also cause spinocerebellar ataxias (SCAs) 15,

[1]Department of Human Genetics, Atomic Bomb Disease Institute, Nagasaki University, Nagasaki 852-8523, Japan. [2]Department of Pharmacy Practice, Nagasaki University Graduate School of Biomedical Sciences, Nagasaki 852-3131, Japan. [3]Department of Cell Regulation, Nagasaki University Graduate School of Biomedical Sciences, Nagasaki 852-3131, Japan. [4]Department of Tumor and Diagnostic Pathology, Atomic Bomb Disease Institute, Nagasaki University, Nagasaki 852-8523, Japan. [5]Gene Research Center, Center for Frontier Life Sciences, Nagasaki University, Nagasaki 852-8523, Japan. [6]Department of Pediatrics and Neonatology, Nagoya City University Graduate School of Medical Sciences, Nagoya 467-8602, Japan. [7]Department of Pediatrics, Hokkaido University Graduate School of Medicine, Sapporo 060-8638, Japan. [8]Department of Medical Genetics, Osaka Women's and Children's Hospital, Osaka 594-1101, Japan. [9]Department of Pediatrics, Todaiji Ryoiku Hospital for Children, Nara 630-8211, Japan. [10]Department of Pediatrics, Fujita Health University School of Medicine, Toyoake 470-1192, Japan. [11]Department of Pathology, Nagasaki University School of Medicine and Graduate School of Biomedical Sciences, Nagasaki 852-8523, Japan.

*Author for correspondence (akino@nagasaki-u.ac.jp)

A.K., 0000-0003-2974-3863; K.O., 0000-0002-1449-5505; K.H., 0000-0002-1594-8334; K.T., 0000-0003-4049-4386; H.M., 0000-0001-5050-2509

Handling Editor: François Guillemot
Received 19 June 2020; Accepted 19 July 2021

Development (2021) 148, dev188755. doi:10.1242/dev.188755

16 and 29, in which aniridia has never been observed (Iwaki et al., 2008; Synofzik et al., 2011; Huang et al., 2012; Sasaki et al., 2015). Abnormal calcium channel function reportedly leads to ataxia in both GLPS and SCA; however, the mechanisms by which the calcium channel protein on the ER causes aniridia only in GLSP are unclear.

We hypothesized a new function of ITPR1 in eye development, in addition to it being a calcium channel. Here, we provide evidence of an ocular-specific isoform of *Itpr1* and demonstrate that disruption of *Itpr1* leads to iris and corneal dysplasia. Although the pathogenic mechanism remains unclear, there is a possibility that ITPR1 regulates the nuclear entry of mechanosensitive transcriptional regulators.

RESULTS

De novo mutations in *ITPR1* cause Gillespie syndrome

Five individuals with GLSP and their healthy parents participated in this study after providing written informed consent (GLSP families 1-5). All individuals with GLSP manifested ataxia and aniridia (Fig. 1A,B). Using whole-exome sequencing, two *de novo* missense mutations and a recurrent in-frame deletion mutation in *ITPR1* (NM_001168272) were identified in GLSP families 1-4. Based on the human GRCH37/hg19 assembly, the mutations were designated as chr3:4,859,894G>A (c.7951G>A; p.G2651R) in GLSP family 1, chr3:4,856,836T>C (c.7756T>C; p.F2586L) in GLSP family 2 and chr3:4,856,866delAAG> (c.7786_7788delAAG; p.K2596del) in GLSP families 3 and 4. Using Sanger sequencing, we also identified a *de novo* mutation in *ITPR1*, chr3:4,856,205G>A (c.7615G>A; p.G2539R), in GLSP family 5 (Fig. 1C). These mutations were absent in our in-house datasets and available public databases, such as dbSNP135, Complete Genomics 69 Genomes, ESP5400 Exome Sequencing Project and 1000 Genomes.

ITPR1 is a giant tetrameric calcium channel protein with six transmembrane domains located in the ER membrane. The Ensembl database (http://www.ensembl.org; Yates et al., 2019) contains various human *ITPR1* transcripts, the longest of which comprises 61 exons and encodes 2743 amino acid residues (NM_001168272.1 and NP_001161744 in GenBank). Detailed structural analyses of rat Itpr1 at near-atomic resolution revealed that this protein contains 106 α-helices (Fan et al., 2015). All mutated amino acids in ITPR1 were positioned in the region between α-helices 101 and 105, which contained the last transmembrane domain and helix linker domain (Fig. 1C). Furthermore, all mutated residues have been evolutionarily conserved, from nematodes to humans and among ITPR family members, which suggests the functional importance of these residues in the structure and function of ITPR1 (Fig. 1D).

Itpr1 expression in the eye

According to the Human Protein Atlas (https://www.proteinatlas.org; Uhlén et al., 2015), *ITPR1* is ubiquitously expressed in human organs, including the eye. To visualize Itpr1 expression in the ocular tissues, we generated genetically modified mice harboring a V5-tag in-frame at the 3′-terminus of *Itpr1* (*Itpr1*^{V5}, Fig. S1A). We performed immunohistochemical experiments with rabbit monoclonal anti-V5 antibody on the eye sections from this knock-in mouse.

First, we tested the specificity of the anti-V5 antibody on eye sections from the *Itpr1*$^{V5/V5}$ mouse at postnatal days 7 and 14 (P7 and P14). Positive signals were observed in the ciliary body, iris and cornea with the V5 antibody, but not with the rabbit IgG negative control (Fig. 2A-D; Fig. S1B,C). Additionally, immunofluorescence staining with the V5 antibody revealed that Itpr1 was expressed in the iris stroma, sphincter and dilator muscles, ciliary body unpigmented epithelium, angle mesenchyme, corneal endothelium and stroma, and hyaloid vessels (Fig. 2E-H). Consequently, it was reasonable to assume that *ITPR1* mutations result in aniridia in individuals with GLSP.

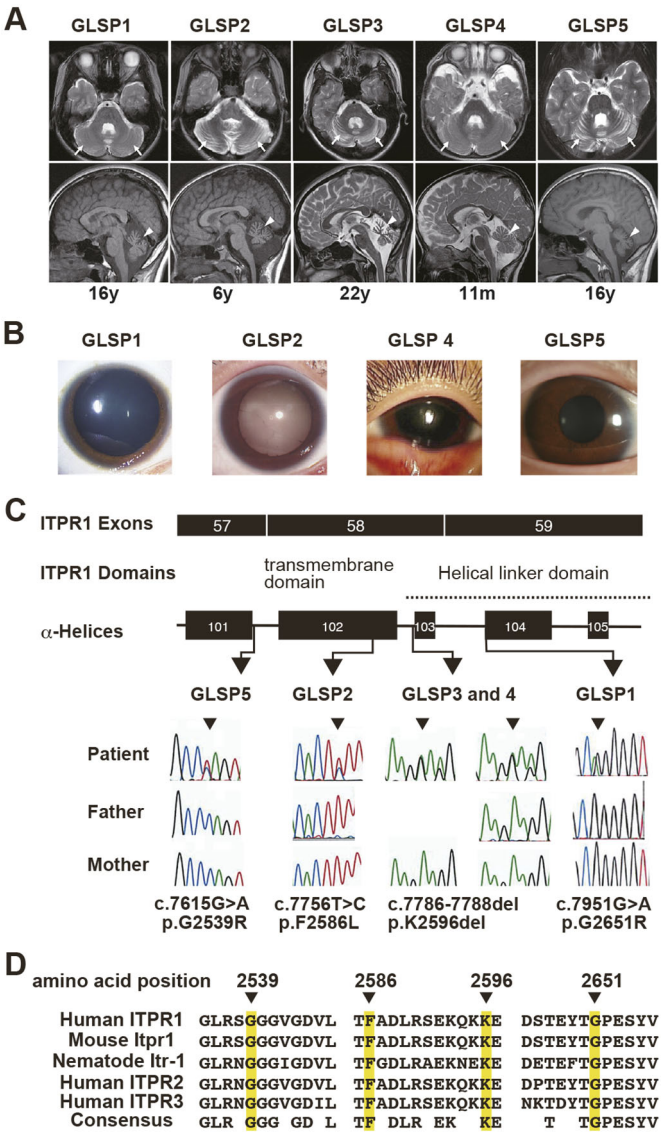

Fig. 1. Symptoms of individuals with GLSP, location of the mutated amino acids and evolutionary conservation of *ITPR1*. (A) Brain magnetic resonance imaging of five individuals with GLSP (GLSP 1-5). Arrows and arrowheads indicate the areas of the brain affected. (B) Aniridia in patients 1, 2, 4 and 5 with GLSP. (C) *De novo* mutations in the C terminus of *ITPR1* in GLSP family members. In GLSP families 1-5, independent *de novo* mutations occurred in exons 57-59 of human *ITPR1*, which comprises 61 exons. These locations correspond to α-helices 101-105 of human ITPR1, which are part of the transmembrane and helical linker domains. (D) Amino acid conservation in nematodes, mice and humans and in other members of the ITPR family.

A novel *Itpr1* transcription start site identified using RNA-sequencing

Mutations or deletions in the anterior half of *ITPR1* result in autosomal-dominant neurological disorders, namely SCAs 15, 16 and 29; however, individuals with SCA do not exhibit aniridia (Iwaki et al., 2008; Synofzik et al., 2011; Huang et al., 2012; Sasaki et al., 2015). Moreover, the *de novo* mutations found in our patients

Development (2021) 148, dev188755. doi:10.1242/dev.188755

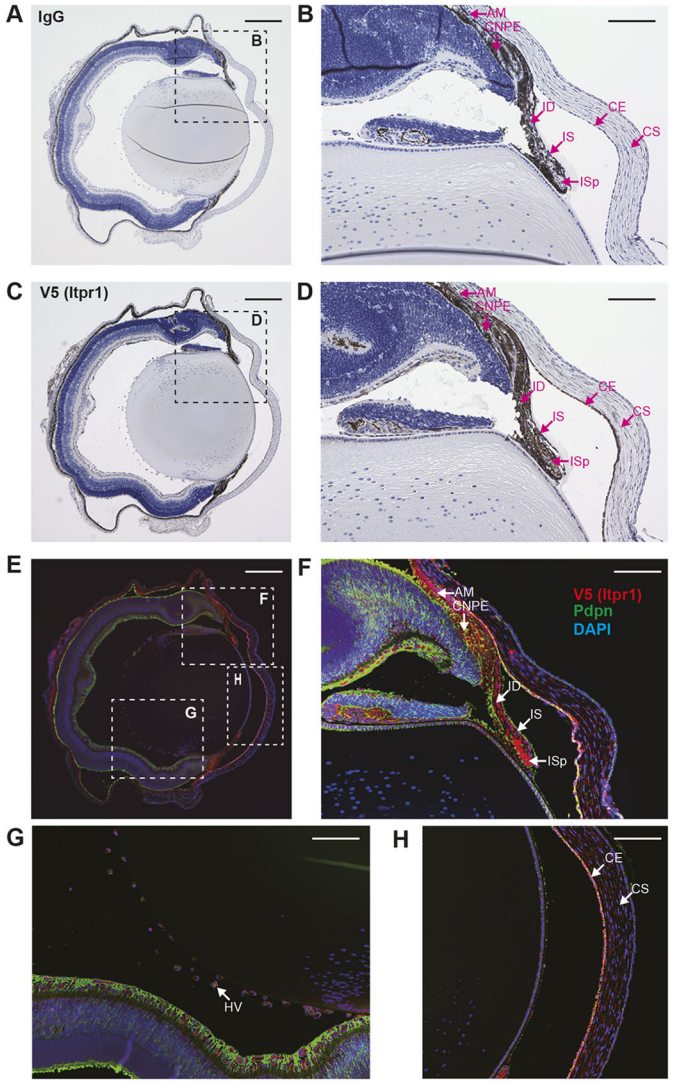

Fig. 2. Itpr1 distribution in the mouse eye. (A) Immunohistochemistry with normal rabbit IgG as a negative control in *Itpr1*$^{V5/V5}$ mouse eye at P7. (B) Magnified view of boxed area in A. (C) Immunohistochemistry with a rabbit monoclonal anti-V5 antibody in *Itpr1*$^{V5/V5}$ mouse eye at P7. (D) Magnified view of boxed area in C. (E) Double immunofluorescence staining with anti-V5 tag antibody (red) and Pdpn (green) in *Itpr1*$^{V5/V5}$ mouse eye at P7. (F) Magnified view of boxed area in E. (G) Magnified view of boxed area in E. (H) Magnified view of boxed area in E. Scale bars: 300 µm in A,C and E; 100 µm in B, D and F-H. AM, angle mesenchyme; CE, corneal endothelium; CNPE, ciliary nonpigmental epithelium; CS, corneal stroma; HV, hyaloid vessel; ID, iris dilator muscle; IS, iris stroma; ISp, iris sphincter muscle.

with GLSP clustered in the 3′-coding region (Fig. 3A). Therefore, we hypothesized that an undiscovered TSS may be present near the 3′ end of *ITPR1*. To confirm this, we performed RNA-sequencing (RNA-seq) using total RNA extracted from the eyes and brains of *Itpr1*$^{V5/V5}$ mice at P0 (Fig. S2A). RNA-seq demonstrated that the number of reads increased remarkably only in the eye at GRCm38/mm10 chr6:108,517,585 in exon 57 of *Itpr1* (Fig. 3B; Fig. S2B). This position corresponded to GRCh37/hg19 chr3:4,854,885, that is, exon 56 of human *ITPR1* (Fig. 3C). No extra exons were identified using RNA-seq and 3′ rapid amplification of cDNA ends. Thus, the transcript from the novel transcription start site (TSS) comprises the last six exons of *Itpr1*.

MAF participates in transcription from the novel *Itpr1* TSS

The UCSC Genome Browser based on GRCh/hg19 showed that the TSS upstream sequence chr3:4,854,530-4,854,885 was conserved among 100 vertebrate species and showed nearly 90% similarity between humans and mice (Fig. S3). The PAX6-binding motif is positioned in the vicinity of the 5′ end of the novel TSS, chr3:4,854,739-4,854,759 (Fig. 3D; Fig. S3). To determine whether the sequence around the novel TSS possesses transcriptional activity, a reporter assay was performed. Reporter vectors containing DNA fragments with or without a PAX6-binding site were transfected into the human embryonic kidney (HEK) 293T cell line (Fig. 3D). Clones 1-5 induced robust reporter activity, although the fragment containing the PAX6-binding site without the sequence proximal to the TSS, clone 6, failed to increase transcription (Fig. 3E). These results suggest that PAX6 is not necessary for transcription from the TSS of *ITPR1*. Given that various TFs (other than PAX6) participate in eye development, *PAX6*, *PAX6(5a)*, *PITX3* and *MAF* cDNAs were cloned into expression vectors with an N-terminal 3×FLAG-tag, and each expression vector was co-transfected with reporter clone 2. *MAF* dramatically enhanced the transcriptional activity (Fig. 3F). Additionally, other TFs (*FOXC1*, *FOSL2*, *OTX1*, *MSX1* and *PITX2*) were also analyzed; however, these did not induce reporter activity to the same extent as *MAF* (Fig. S4).

Clones 7 and 8, without the proximal region and PAX6-binding domain, notably increased the reporter activity (Fig. 3D). We sought to detect MAF-binding sites using VISTA (http://genome.lbl.gov/vista/index.shtml; Mayor et al., 2000), an online tool to predict TF-binding motifs depending on the evolutionary conservation among species, and identified three potential MAF-binding sites tandemly positioned within clone 8, chr3:4,854,530-4,854,664 (Fig. S4B). Wild-type MAF greatly increased the reporter activity of clone 8, whereas the MAF mutant, R288P, which had been identified in individuals with ocular diseases, failed to do so (Fig. 3G; Anand et al., 2018). To determine whether MAF associates with these motifs *in vitro*, 3×FLAG-tagged MAF and the mutant R288P were incubated with magnetic nanobeads conjugated with double-stranded oligonucleotides with the MAF-binding motif and immunoblotted with an anti-FLAG (DDDDK) antibody. This assay demonstrated that MAF showed direct binding with each MAF-binding motif; however, the R288P mutant showed weak binding (Fig. S4C). Additionally, a chromatin immunoprecipitation (ChIP) assay revealed that the wild-type MAF bound to the motifs with higher strength compared with the R288P mutant (Fig. 3H).

To explain the significant reduction in reporter activity in clone 6, including MAF-binding sites, we hypothesized that some TFs suppressed the reporter activity by competing with it in that region to occupy the binding motif. Using the JASPAR database (http://jaspar.genereg.net; Sandelin et al., 2004), inverted overlapping SOX9-binding motifs were detected in GRCh37/hg19 chr3:4,854,734-4,854,742 (sense) and 4,854,731-4,854,739 (antisense), which involved adjustments to the PAX6-binding motif (Fig. 3I). The binding of SOX9, an NCC marker, to these motifs was demonstrated by a ChIP assay using the mouse cranial neural crest cell line O9-1 (Fig. 3J). Wild-type SOX9 with a FLAG tag showed binding with the SOX9 motifs, whereas the H165Q mutant showed a lower binding capacity compared with the wild type (Fig. S4D). We also observed that SOX9 neutralized the increase in transcriptional activity that was induced by MAF (Fig. 3K).

Development (2021) 148, dev188755. doi:10.1242/dev.188755

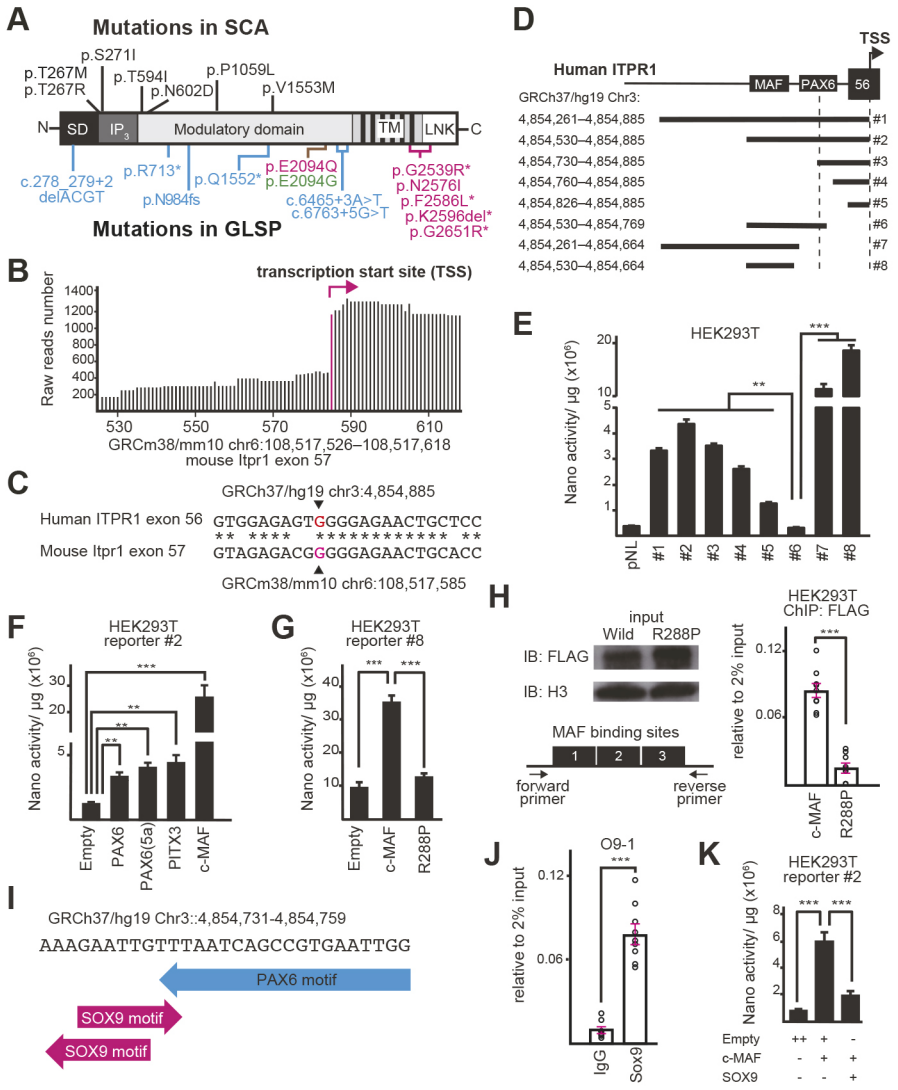

Fig. 3. Eye-specific novel TSS and regulation by MAF and SOX9. (A) Distribution of GLSP mutations and mutations identified in individuals with spinocerebellar ataxia (SCA). Hereditary forms of GLSP mutations are classified by color: magenta, *de novo*; green, autosomal-dominant; and light blue, autosomal-recessive. The mutations identified in this study are indicated by an asterisk. SCA mutations have been reported by Sasaki et al. (2015). (B) The raw number of mapped RNA-seq reads of mouse eye at P0 on GRCm38/mm10 chr6:108,517,526-108,517,618, exon 57 of *Itpr1*. The magenta bar indicates the eye-specific TSS. (C) Comparison of human and mouse sequences around the novel TSS. The magenta and red characters indicate the TSS in human and mouse, respectively, and the asterisks indicate the amino acids common to both sequences. (D) DNA fragments were cloned into a reporter vector (pNL1.1), resulting in clones 1-8. The indicated genomic positions are based on the human genome GRCh37/hg19. The PAX6- and MAF-binding motifs are indicated as boxes. (E) Relative nanoLuc luciferase (NLuc) activities in HEK293T cells transfected with the different deletion constructs (clones 1-8) shown in D. Total NLuc activity was divided by the total amount of protein for normalization. $^{**}P<0.01$, $^{***}P<0.001$, post hoc Dunnett's test, $n=9$. (F) Relative NLuc activities in HEK293T cells transduced with clone 2 in combination with each TF. $^{**}P<0.01$, $^{***}P<0.001$, two-tailed Student's *t*-test, $n=9$. (G) Induced transactivation of clone 8 by the wild-type MAF and R288P mutant. $^{***}P<0.001$, two-tailed Student's *t*-test, $n=9$. (H) ChIP assay of MAF binding in HEK293T cells. To confirm the expression of wild-type and R288P mutant MAF, the retrieved chromatin solution was used for immunoblotting using an anti-FLAG antibody and H3 as an internal control. The binding capacity was quantified using quantitative PCR. The *y*-axis represents the amount of immunoprecipitated DNA relative to the total amount of 2% input DNA. $^{***}P<0.001$, two-tailed Student's *t*-test, biological replicates ($n=3$) with three technical replicates. (I) SOX9-binding motifs adjacent to the PAX6-binding site in D. (J) ChIP assay of Sox9 binding in the mouse neural crest cell line O9-1. $^{***}P<0.001$, two-tailed Student's *t*-test, biological replicates ($n=3$) with three technical replicates. (K) Neutralization of MAF-induced transcriptional activity by SOX9. Plus sign indicates 0.25 µg of expression vector. $^{***}P<0.001$, two-tailed Student's *t*-test, $n=9$. IP_3, IP_3 binding domain; LNK, helix linker domain; SD, suppressor domain; TM, transmembrane domain.

An ocular-specific transcript encodes a transmembrane protein consisting of only 218 amino acid residues

The short *Itpr1* transcript comprises several open reading frames; however, the longest one consists of 218 amino acid residues (hereafter referred to as the 218-aa isoform) and contains all the relevant mutations detected in the patients with GLSP included in our study (Fig. 4A). To determine the nature of the protein encoded by this transcript, cDNA fragments containing exons 57-62 of *Itpr1* with a V5 tag sequence at the 3′ end were cloned into an expression vector and transfected into HEK293T cells. This construct produced three protein bands with molecular weights (MWs) of 30, 25 and 20 kDa; the 20 kDa band corresponded to a peptide of 175 amino acids (Fig. 4B). The upper two bands disappeared upon mutagenesis, which removed the first methionine

Development (2021) 148, dev188755. doi:10.1242/dev.188755

residue of the 218-aa isoform. The 25 kDa band coincided with the expected MW of the 218-aa isoform, whereas the identity of the 30 kDa band was unknown. We hypothesized that the higher-molecular-weight protein was a post-translationally modified 218-aa isoform. We did not observe any changes upon phosphatase treatment. We then screened *N*-acetylglucosamine (GlcNAc)-binding motifs (Asn-X-Ser/Thr) and found two putative GlcNAc-binding sites, asparagine residues at positions 91 and 179, in the 218-aa isoform. Substitution of asparagine for lysine at position 91 in the 218-aa isoform (N91K) resulted in loss of the 30 kDa band, whereas substitution of asparagine for lysine at amino acid position 179 (N179K) did not have an effect (Fig. 4C). Treatment with EndoH glycosidase, which removes oligosaccharides from *N*-linked glycoproteins, also resulted in the loss of the 30 kDa band, similar to that observed in the N91K mutant (Fig. S5A).

The 218-aa isoform was expected to contain a single ER transmembrane domain (Fig. 4A); therefore, we attempted to determine the intracellular localization of this protein. Immunoblotting assays using cellular fractions of HEK293T cells transfected with 218-aa-V5-expressing vectors revealed that the protein was localized in the membrane and nuclear fraction and that the K71Del mutation did not affect the localization (Fig. 4D).

The 218-aa isoform is expressed in the eye corresponding to AES formation

To confirm the existence of the 218-aa isoform in the eye, total protein samples were extracted from the eyes of *Itpr1*$^{+/+}$ and *Itpr1*$^{V5/V5}$ mice and then immunoblotted. A weak band of 27 kDa corresponding to the 218-aa isoform was detected in the protein fraction from the eye of *Itpr1*$^{V5/V5}$ mice, but not in that from *Itpr1*$^{+/+}$ mice (Fig. 4E).

We examined the serial expression of the 218-aa isoform of Itpr1 in the eye according to the developmental stage. We found that this isoform began to be expressed at a very low level at embryonic day (E) 13 and that its expression was abundant during the formation of AES; however, this expression was not detected in the brain (Fig. 4F,G; Fig. S5B). Western immunoassay analysis of proteins extracted from multiple tissues at E18 and P7 revealed that this form was only expressed in the eye (Fig. 4H; Fig. S5C). Sox9 suppressed transcription of a novel TSS (Fig. 3I-K). Furthermore, Sox9

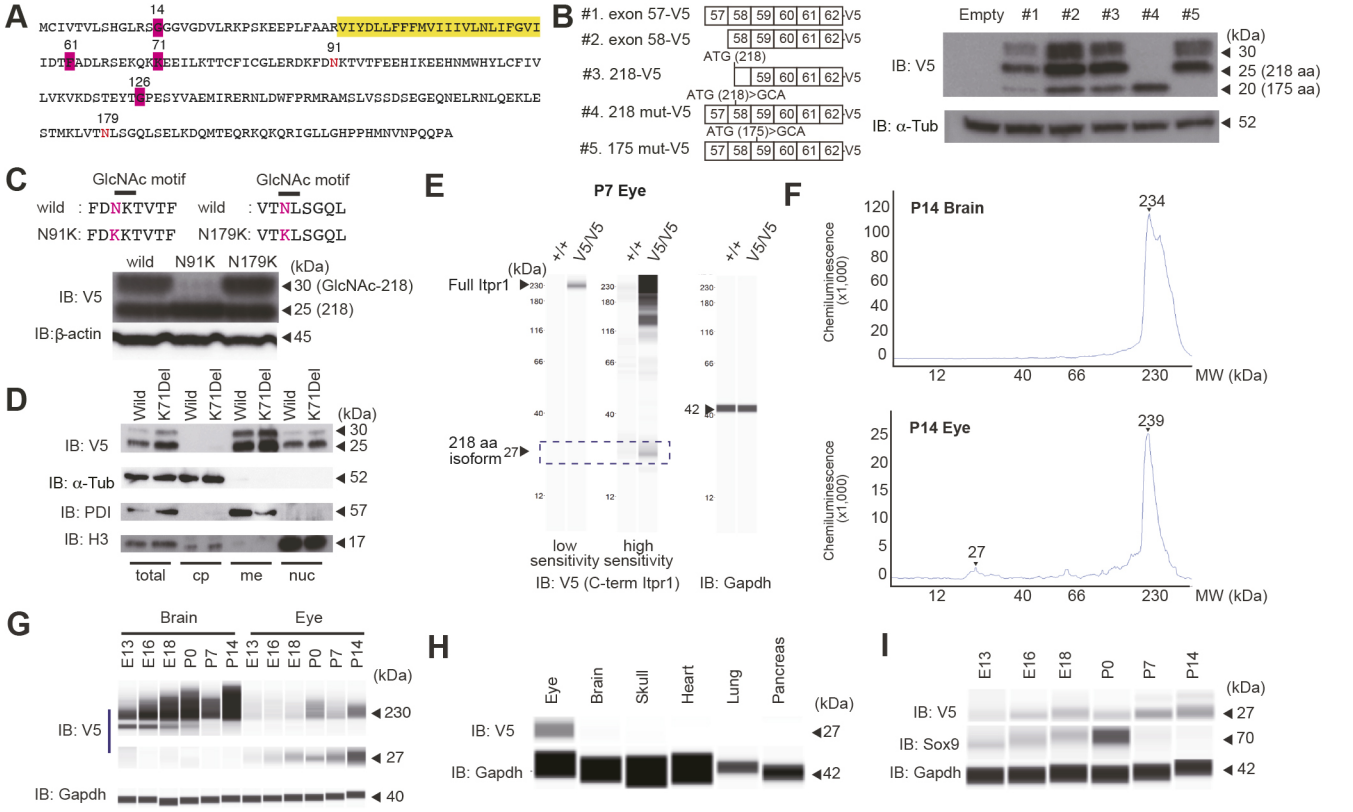

Fig. 4. An Itpr1 isoform comprising 218 amino acid residues is localized in the ER. (A) Amino acid sequence of the 218-aa isoform of mouse Itpr1. GLSP mutations in this study and the Itpr1 transmembrane domain are highlighted in magenta and yellow, respectively. Asparagine (N) residues at positions 91 and 179 are shown in red (see Fig. 3C,D). (B) Cytomegalovirus (CMV) promoter-driven constructs expressing various types of mouse Itpr1 with a C-terminal V5 tag. Immunoblot with an anti-V5 tag antibody is presented on the right. α-Tubulin (α-Tub) was used as an internal control. (C) Two predicted GlcNAc-binding motifs at positions 91 and 179. N was replaced with lysine (K) by PCR-based mutagenesis in each mutant construct. Wild-type and N79K and N179K mutants of the 218-aa Itpr1 isoform were expressed in HEK293T cells, and cell extracts were then used for immunoblotting. β-Actin was used as an internal control. (D) Fractions of HEK293T cells transfected with wild-type or K71Del mutant constructs were used for immunoblotting. Cell fractions were confirmed by immunoblotting with the following control antibodies: α-Tub for the cytoplasm, PDI for the ER membrane and H3 for the nuclear fraction. (E) Immunoassays of brain and eye extracts from *Itpr1*$^{+/+}$ and *Itpr1*$^{V5/V5}$ mice at P7 performed with a rabbit monoclonal anti-V5 antibody that recognizes the Itpr1 C terminus. Staining for glyceraldehyde-3-phosphate (Gapdh) was used as a loading control (red arrowhead). (F) Electropherograms of capillary western immunoassays using brain (top) and eye (bottom) samples at P14. (G) Western immunoassay of brain and eye extracts from *Itpr1*$^{V5/V5}$ mice of different ages between E13 and P14 performed with an anti-V5 antibody and an anti-Gapdh antibody. (H) Immunoassays of extracts from *Itpr1*$^{V5/V5}$ mouse tissues at P7 with an anti-V5 antibody. (I) Immunoassay of extracts from an *Itpr1*$^{V5/V5}$ mouse eye at each age using antibodies against V5, Sox9 and Gapdh. cp, cytoplasm; me, biological membrane; nuc, nuclear fraction that included the nuclear membrane.

Development (2021) 148, dev188755. doi:10.1242/dev.188755

expression decreased after birth, which corresponded to the formation of AES (Fig. 4I).

Loss of Itpr1 causes ataxia and failure of AES development

We attempted to disrupt exon 59 of mouse *Itpr1* (NM_010585) corresponding to exon 58 of human *ITPR1*, which includes two mutations, p.F2586L and p.K2596del, using the CRISPR/Cas9 method (Fig. S6A). Three founder mice with a deletion in exon 59 at a high mosaic rate died soon after birth for unknown reasons. Histological analysis revealed that the *Itpr1*-deficient mice appeared normal (Fig. S6B), because the formation of the AES structures was completed after birth (Hägglund et al., 2017).

Given that almost all *Itpr1*-deficient mice died *in utero* (Matsumoto et al., 1996), we established another mouse line with a seven-base pair deletion (c.8238_8244delAGCCGGC) in the last exon of *Itpr1*, $Itpr1^{\Delta 7bp}$, which resulted in a frameshift and read-through mutation, p.Q2747PfsTer40 (Fig. 5A). In vertebrates with image-forming eyes, the last amino acids of the C-terminal region of ITPR1 are highly conserved. However, the similarity of this sequence between vertebrates and invertebrates, as well as among ITPR family members, was low (Fig. 5B). Western immunoassay analysis with antibodies recognizing 1883-NKKKDDEVDR-DAPSRKKAKE-1902 of Itpr1 revealed that the seven-base pair deletion led to the loss of Itpr1 (Fig. 5C). However, mice homozygous for this mutation survived until weaning (~3 weeks) and exhibited both ataxia and aniridia (Fig. 5D and Movie 1).

We then observed abnormalities of the AES in $Itpr1^{\Delta 7bp/\Delta 7bp}$ mice at P21 using Hematoxylin and Eosin (H&E) staining. In comparison with their $Itpr1^{+/+}$ littermates, $Itpr1^{\Delta 7bp/\Delta 7bp}$ mice showed AES defects, including shrunken iris and reduced corneal thickness; however, no defects in the lens and retina were found (Fig. 5E). The iris of $Itpr1^{\Delta 7bp/\Delta 7bp}$ mice showed a loss of lymphatic vessels in the stroma and dilator muscles, and sparse sphincter muscles. Additionally, these mice developed a reduction in corneal thickness resulting from a compact layer of the stromata and failure of epithelial stratification, and thinner and nonsmooth corneal endothelium (Fig. 5F,G; Fig. S6C). Notably, the iris stroma, corneal stroma and corneal endothelium originate from NCCs (Kikuchi et al., 2011). In addition, we found that $Itpr1^{+/\Delta 7bp}$ mice did not show aniridia or AES defects (Fig. S6D).

Failure of AES development and the presence of undifferentiated NCCs in $Itpr1^{\Delta 7bp/\Delta 7bp}$ mice

In addition to its multipotency, a high migratory capacity is a feature of NCCs. First, we assessed the existence of NCCs in the AES region at P0 in $Itpr1^{\Delta 7bp/\Delta 7bp}$ mice using the p75 neurotrophin receptor (p75NTR), which is an NCC marker (Pan et al., 2016). We observed the presence of p75NTR-positive cells in the iridocorneal region in $Itpr1^{\Delta 7bp/\Delta 7bp}$ mice (Fig. S7A). Furthermore, apoptotic cells were not detected in the AES in mice at P0 (Fig. S7B). Thus, we assumed that aniridia in $Itpr1^{\Delta 7bp/\Delta 7bp}$ mice was caused by the failure of differentiation and not by either NCC migration or apoptosis.

Next, we studied the reason for the loss of *Itpr1*, leading possibly to the failure of AES differentiation. H&E staining indicated the loss of iris stroma and lymphatic vessels in the iris in $Itpr1^{\Delta 7bp/\Delta 7bp}$ mice; therefore, we chose podoplanin (Pdpn) as an iris stromal marker protein (Birke et al., 2010; Kaser-Eichberger et al., 2015). Pdpn is a transmembrane glycoprotein and a marker of lymphatic endothelial cells that participates in cancer metastasis through actin reorganization (Wicki et al., 2006). As expected, Pdpn signals were observed in the iris stroma, lymphatic vessels and sphincter muscles of $Itpr1^{+/+}$ mice. However, the signals were only detected in the iris sphincter muscle of $Itpr1^{\Delta 7bp/\Delta 7bp}$ mice at P21, which indicated dysplasia of the iris stroma and loss of lymphatic vessels (Fig. 6A). Glutamine receptor interacting protein 1 (Grip1), a marker of corneal endothelium (Yoshihara et al., 2015), was selected to visualize the presence of aberrant AES structures in $Itpr1^{\Delta 7bp/\Delta 7bp}$ mice at P21. Similar to the findings described above, there were thick continuous lines of Grip1 signals in the corneal endothelium of $Itpr1^{+/+}$ mice, whereas thin discontinuous lines were observed in that of $Itpr1^{\Delta 7bp/\Delta 7bp}$ mice. Furthermore, Grip1 signals were lost in the iris stroma of $Itpr1^{\Delta 7bp/\Delta 7bp}$ mice at P21, which implies the failure of AES differentiation (Fig. S7C).

Immunofluorescent staining with an anti-α-SMA antibody was also performed to confirm the abnormal structure of the iris sphincter and dilator muscles in $Itpr1^{\Delta 7bp/\Delta 7bp}$ mice at P21. Their dilator muscles were noncontiguous or lost and their sphincter muscles were sparse, as shown by H&E staining and immunostaining (Fig. 5G and Fig. 6B).

We determined the expression of Pdpn and α-SMA from E13 to P7, corresponding to the timing of the elevated expression of the 218-aa isoform in the mouse eye. The expression levels of Pdpn and α-SMA were indistinguishable between $Itpr1^{+/+}$ and $Itpr1^{\Delta 7bp/\Delta 7bp}$ mice by E18, whereas the α-SMA-positive cells, the progenitors of dilator muscle, decreased in $Itpr1^{\Delta 7bp/\Delta 7bp}$ mice at P0. Pdpn decreased in the iris stroma and α-SMA signals were disrupted in $Itpr1^{\Delta 7bp/\Delta 7bp}$ mice, indicating the loss of iris stroma and dilator muscles by P7 (Fig. 6C). Loss of Itpr1, probably the 218-aa isoform, disrupted AES formation after birth. The expression levels of Pdpn and α-SMA were normal in $Itpr1^{+/\Delta 7bp}$ mice (Fig. S7D). Finally, p75NTR-positive cells, most likely undifferentiated NCCs, remained in the iris and corneal stroma, and ciliary body in $Itpr1^{\Delta 7bp/\Delta 7bp}$ mice at P21 (Fig. 6D; Fig. S7E).

The 218-aa isoform interacts with actomyosin filaments and regulates nuclear entry of transcription factors

We confirmed that the 218-aa isoform of Itpr1 was expressed in ocular tissues and localized to the membrane fraction through its transmembrane domain (Fig. 4A,D). However, the mechanism that causes aniridia in individuals with GLSP remains unknown. To investigate this, we characterized ITPR1-associated proteins using mass spectrometry (MS). Cell lysates extracted from the eyes of $Itpr1^{V5/V5}$ mice at P0 were immunoprecipitated with an anti-V5 antibody and separated using SDS-PAGE. Three intense bands at 245, 100 and 45 kDa were visualized using Coomassie Brilliant Blue staining, clipped out of the gel and used for MS (Fig. 7A). MS analysis showed that the 245 kDa band corresponded to non-muscle myosin family members (myosin 9 and 10), the 100 kDa band to actinin and the 45 kDa band to actin family members (β-actin and α-actin). Interaction between the wild-type or K71Del mutant of the 218-aa isoform and actomyosin members was confirmed by immunoprecipitation followed by immunoblotting with anti-β-actin and anti-myosin IIa (myosin 9) antibodies; however, the 218-aa isoforms were incapable of binding to vinculin, a component of focal adhesion (Fig. S8A).

We developed NIH3T3 mouse fibroblast cell lines expressing the wild-type or K71Del mutant of the 218-aa isoform with a V5-tag under treatment with 1 µg/µl doxycycline (Fig. S8B). First, the localization of the 218-aa isoform of Itpr1 was verified using immunofluorescence staining. We chose protein disulfide isomerase (PDI) as an ER marker protein and lamin A/C as a nuclear membrane marker; double immunostaining revealed that both wild-type and K71Del mutants of the 218-aa isoform were localized not

Development (2021) 148, dev188755. doi:10.1242/dev.188755

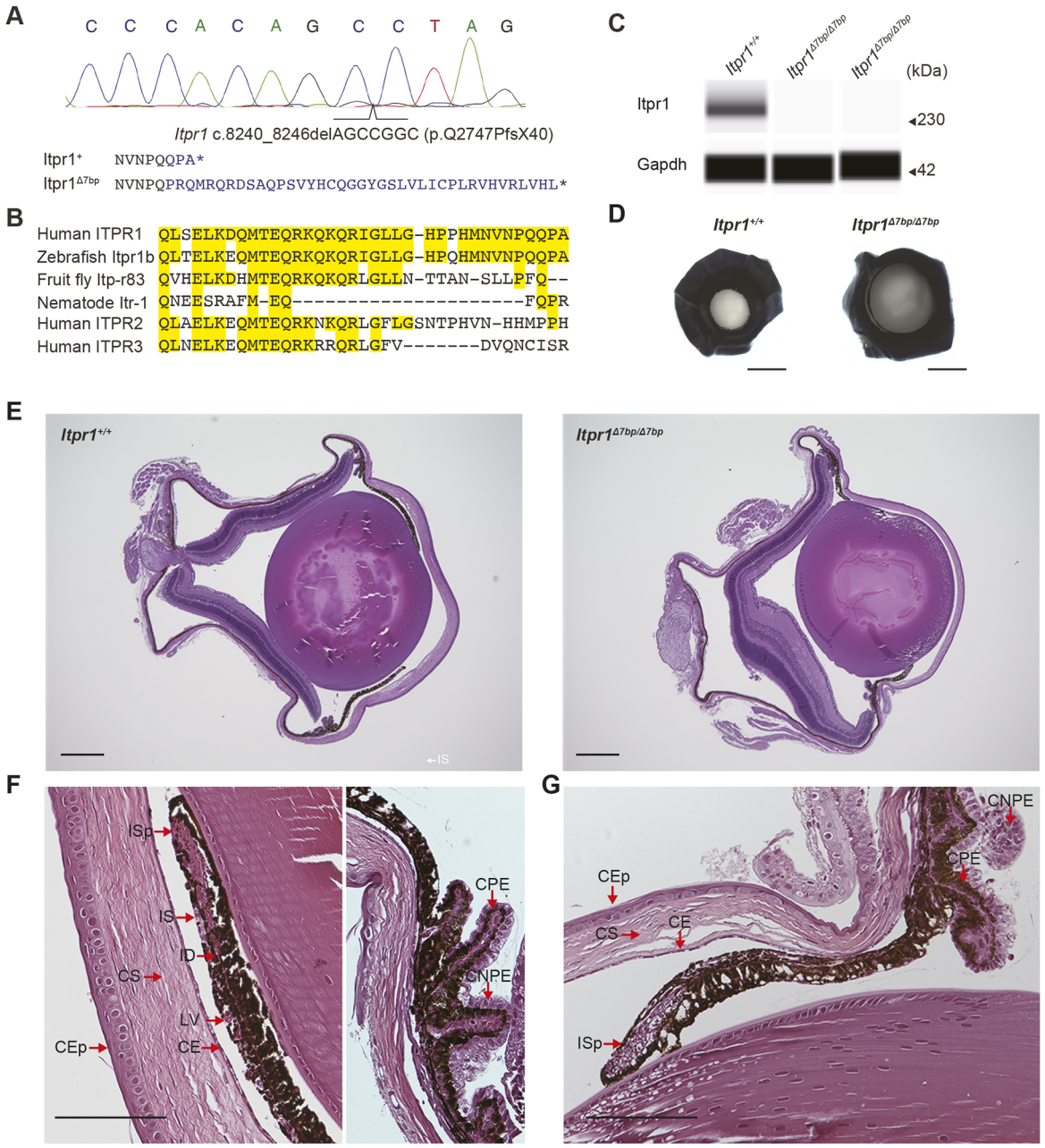

Fig. 5. Defects in neural crest-derived ocular tissues are caused by a seven base pair deletion in the mouse *Itpr1* 3′ terminus. (A) Deletion of seven base pairs in the last *Itpr1* exon c.8240_8246delAGCCGGC resulted in the p.Q2747PfsX40 protein mutation. (B) Similarity of amino acid sequences at the C-terminal end of ITPR1. Highlighted residues indicate amino acids conserved between human ITPR1 and other proteins. (C) Images of immunoassays of brain extracts from *Itpr1*$^{+/+}$ and *Itpr1*$^{\Delta 7bp/\Delta 7bp}$ mice at P21 performed with a rabbit polyclonal anti-Itpr1 antibody that recognizes 1883-NKKKDDEVDRDAPSRKKAKE-1902 of mouse Itpr1. Gapdh was used as a loading control. (D) Frontal views of *Itpr1*$^{+/+}$ mouse eye (left) and *Itpr1*$^{\Delta 7bp/\Delta 7bp}$ mouse eye (right) at P21. (E) H&E staining of eye sections at P21 in the *Itpr1*$^{+/+}$ mouse (left) and *Itpr1*$^{\Delta 7bp/\Delta 7bp}$ mouse (right). (F) Magnified images of *Itpr1*$^{+/+}$ mouse showing the cornea and tip of iris (left) and ciliary body (right). (G) Magnified image of *Itpr1*$^{\Delta 7bp/\Delta 7bp}$ mouse. Scale bars: 1 mm in D; 300 µm in E; 100 µm in F,G. CE, corneal endothelium; CEp, corneal epithelium; CNPE, ciliary nonpigmental epithelium; CPE, ciliary pigmental epithelium; CS, corneal stroma; ID, iris dilator muscle; IS, iris stroma; ISp, iris sphincter muscle; LV, lymphatic vessel.

only in the ER, but also in the nuclear and cytoplasmic membranes (Fig. 7B; Fig. S8C).

An immunofluorescence assay using phalloidin also revealed that the wild-type isoform of Itpr1 was associated with unidirectional actin filaments; conversely, the mutant isoform caused a radial arrangement of actin fibers (Fig. 7C,D). To visualize the morphology of actin fibers in AES tissues, we performed immunostaining with an anti-β-actin antibody on the sections of the eye at P21. Strong striated signals were observed in the iris and cornea in *Itpr1*$^{+/+}$, but fewer and weaker signals were found in the iris and corneal stroma in *Itpr1*$^{\Delta 7bp/\Delta 7bp}$ (Fig. 7E).

Given that the proteins that were immunoprecipitated with Itpr1, namely, actin, myosin and actinin, are components of focal adhesions, we examined the shape and configuration of focal adhesions in each cell line using an anti-vinculin antibody. Focal adhesions were arranged in a unidirectional pattern in the cells

Development (2021) 148, dev188755. doi:10.1242/dev.188755

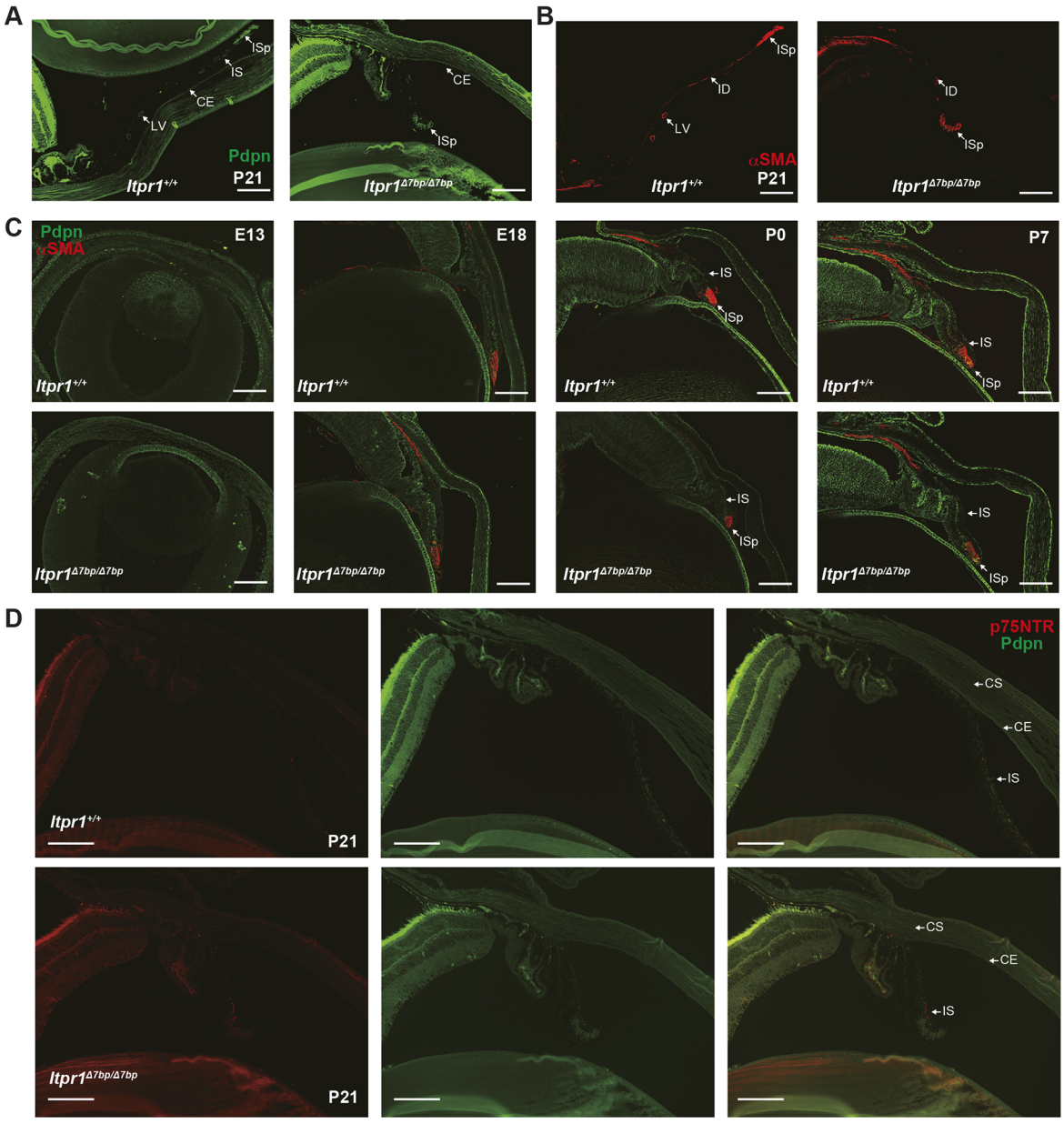

Fig. 6. Developmental failure of iris and cornea in *Itpr1*$^{\Delta 7bp/\Delta 7bp}$ mice. (A) Immunostaining of Pdpn (green) at P21. (B) Immunostaining of α-Sma (red) at P21. (C) Iris development from E13 to P7 using anti-Pdpn (green) and anti-α-Sma (red) antibodies. (D) Double immunofluorescence staining of p75NTR (red) and Pdpn (green) at P21. Scale bars: 100 µm. α-Sma, α-smooth muscle actin; CE, corneal endothelium; CS, corneal stroma; ID, iris dilator muscle; IS, iris stroma; ISp, iris sphincter muscle; LV, lymphatic vessel.

expressing the wild-type 218-aa isoform, whereas the K71Del mutant showed long, narrow, radially arranged adhesions (Fig. 7F, Fig. S8D). The focal adhesion signal intensity was quantified using vinculin antibodies, and the signal intensity in the wild type was significantly higher than in the K71Del mutant (Fig. 7G).

A mechanosensitive transcriptional regulator, Yes-associated protein (YAP), regulates the development of craniofacial structures derived from NCCs (Wang et al., 2016). In addition, nuclear translocation of YAP is induced by mechanical forces generated by extracellular matrix stiffness, stress fibers and focal adhesions (Dupont et al., 2011; Elosegui-Artola et al., 2017). Nuclear Yap translocation was quantified by immunofluorescence and western immunoassays. The signal intensity of Yap in the nucleus of wild type-expressing cells was significantly higher than that of the deletion mutant-expressing cells (Fig. 7H,I). We performed a scratch assay to compare the motility of the two cell lines but found no difference (Fig. S8E).

DISCUSSION

Although *ITPR1*, a causative gene of SCA, is not associated with aniridia, independent studies have reported that mutations in this gene cause GLSP characterized by aniridia and ataxia (Gerber et al., 2016; McEntagart et al., 2016; Dentici et al., 2017; Carvalho et al., 2018; Paganini et al., 2018). However, the pathogenic mechanisms of aniridia and the reasons underlying its occurrence solely in individuals with GLSP remain unclear. Against this background, we identified an ocular-specific *Itpr1* transcript encoding 218 amino acid residues (218-aa isoform), as a key molecule in AES development and established a GLSP model mouse, *Itpr1*$^{\Delta 7bp/\Delta 7bp}$, which displays developmental failure of AES.

Development (2021) 148, dev188755. doi:10.1242/dev.188755

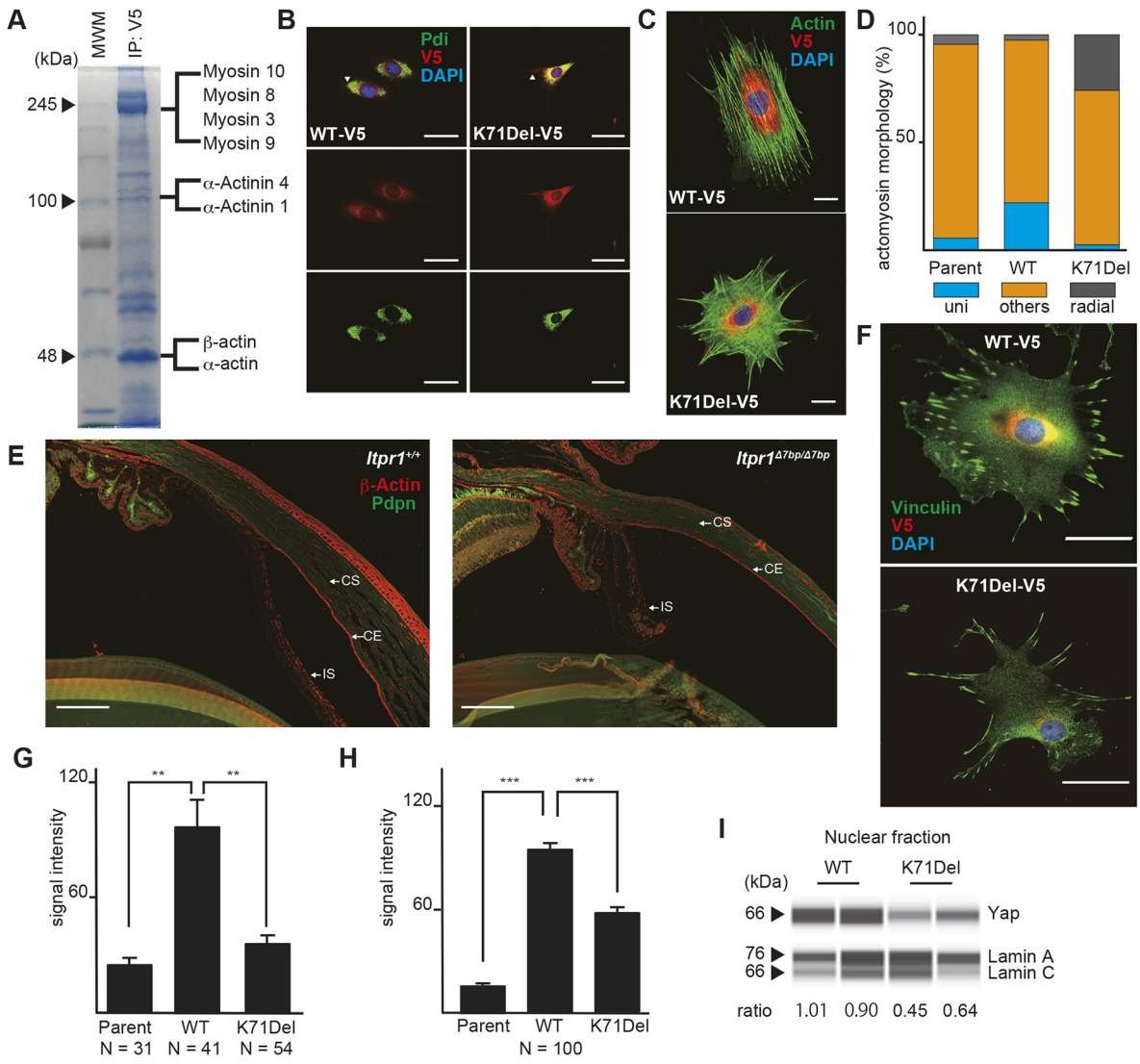

Fig. 7. Itpr1 218-aa isoform binds to actomyosin filaments and regulates the direction of stress fibers and focal adhesion. (A) Coomassie Brilliant Blue staining of proteins immunoprecipitated with a mouse monoclonal anti-V5 antibody. Proteins of 245, 100 and 45 kDa were subjected to MS. (B) Localization of the 218-aa isoform on the ER membrane. Green indicates Pdi, an ER marker, whereas red indicates V5-tagged 218-aa isoforms. White triangles indicate the localization on the plasma membrane. The wild-type 218-aa isoform is shown on the left and the K71Del mutant on the right. (C) Immunofluorescence images of actin filaments in NIH3T3 cells. Actin filaments visualized with phalloidin (green) and anti-V5 antibody indicating V5-tagged 218-aa isoforms (red) in wild type (top) and K71Del mutants (bottom). (D) Evaluation of the actomyosin morphology. The unidirectional filament is shown in light blue, radially arranged filament in gray, and others in orange; *n*=200 each. Parent indicates NIH3T3. (E) Double immunostaining of β-actin (red) and Pdpn (green) at P21. (F) Immunofluorescence images of focal adhesions in NIH3T3 cells, showing vinculin (green) and V5-tagged 218-aa isoforms (red) in wild-type 218-aa isoforms (top) and K71Del mutants (bottom). (G) Fluorescence intensity of vinculin. ***P*<0.01, two-tailed Student's *t*-test. (H) Nuclear signal intensity of Yap. ****P*<0.001, two-tailed Student's *t*-test; *n*=100 each. (I) Immunoassay of nuclear fraction proteins with Yap and lamin A/C, a nuclear marker. Ratio indicates the value of signal intensity of Yap divided by that of lamin A/C. Scale bars: 30 µm in C; 50 µm in B,F; 100 µm in D.

Novel function of ITPR1 in AES formation, in addition to its function as a calcium channel

ITPR1 is a ubiquitously expressed giant calcium channel that regulates calcium ion release from the ER in an IP_3 binding-dependent manner. Calcium ions play important roles in neural activity and muscle contraction; therefore, it is reasonable that aberrant ITPR1 function causes SCA and aniridia. Adult mice harboring the C1976Y mutation in *Itpr1* have been reported to exhibit dysfunction in the contraction of the iris constrictor muscles (Chen et al., 2020). However, this result is insufficient to explain why aniridia develop only in individuals with GLSP.

In the current study, we found a mutation hotspot in individuals with GLSP and a novel TSS in exon 57 of murine *Itpr1*, which corresponds to exon 56 of human *ITPR1*. Transcripts transcribed from the TSS encoded only 218 amino acid residues but contained all the identified *de novo* GLSP mutations. As a complement to the novelty of the TSS, the latest version of DBTSS (https://dbtss.hgc.jp; Suzuki et al., 2018) suggests the existence of this TSS in the adult human brain; however, the transcript and its translated product have not been identified *in vivo*; therefore, this is the first report to reveal its existence. Immunoblotting assay revealed that the 218-aa isoform increased in

Development (2021) 148, dev188755. doi:10.1242/dev.188755

an eye-specific manner from E13 to P14, coinciding with the period of AES development in mice.

Our experiments using doxycycline-inducible cell lines demonstrated that the 218-aa isoform affected actomyosin filament and focal adhesion, and *Itpr1*$^{\Delta 7bp/\Delta 7bp}$ mice displayed shredded actin fibers in the iris and corneal stroma. Mutations in the actin and non-muscle myosin family members cause eye malformations in humans and mice (Rivière et al., 2012; Samuels et al., 2013). These findings suggest that the ITPR1-actomyosin-focal adhesion network might be required for ocular development. Given that Yap nuclear localization was higher in the wild type of 218 aa isoform-expressing cells than in the K71Del mutant-expressing cells, it is possible that the mechanical force generated by the network induces nuclear translocation of YAP or another transcriptional regulator in developing AES tissues. The involvement of the ITPR1-actomyosin-focal adhesion network in the differentiation of AES is an excellent target for regenerative medicine, and further studies in this area are warranted. In addition, the cGMP kinase signaling complex, which includes ITPR1 as a component, interacts with actin (Schlossmann et al., 2000; Koller et al., 2003), and this interaction might play a role in AES formation.

The C terminus of ITPR1 is essential for AES development

Our *Itpr1*-deficient mice with a frameshift mutation in exon 59 died soon after birth and exhibited no overt eye abnormalities, similar to the mice established by McEntagart et al. (2016). *Itpr1*$^{\Delta 7bp/\Delta 7bp}$ mice survived until their weaning date, developed ataxia and failed to form AES tissues. This implies that the C terminus of ITPR1 has an unknown function evolutionarily in the differentiation into AES tissues. For instance, a homology search using BLASTP in NCBI (https://blast.ncbi.nlm.nih.gov/Blast.cgi; Altschul et al., 1990) predicted that the last 32 amino acids of ITPR1 (2712-LKDQMTEQRKQKQRIGLLGHPPHMNVNPQQPA-2743) are homologous to the prohead core protein serine protease, an uncharacterized peptidase from the S77 superfamily. Consequently, we conclude that the C terminus of ITPR1, probably the 218-aa isoform, contributes to the differentiation into AES tissues.

Competition between MAF and SOX9 regulates AES formation via the 218-aa isoform

Complex interactions between TFs and their targets regulate the development of the AES. PAX6, a master regulator of ocular development, did not activate transcription from the TSS identified in this study, whereas MAF greatly enhanced the transcription. These results indicate that the eye-specific expression of the 218-aa isoform of *ITPR1* induced by the direct binding of MAF leads to the differentiation of AES from NCCs. Given that MAF contributes to the late differentiation of several tissues and cells, such as lenses and chondrocytes (Kim et al., 1999; MacLean et al., 2003), it might also participate in the late differentiation of AES.

However, SOX9, a marker of NCCs and bound downstream of the MAF-binding motifs, suppressed the expression of the novel transcript. Sox9 disappeared in a stepwise fashion through the process of differentiation into AES tissues. Competition between SOX9 and MAF contributes to AES formation, probably in cooperation with other TFs.

Are AES tissues derived from NCCs or mesoderm?

Our knowledge of the differentiation of NCCs into AES tissues is based on transplantations between chicken and quail embryos (Johnston et al., 1979). Using these animal models, it has been shown that AES tissues, such as corneal stroma and endothelium, iridial stroma and pericytes are of NCC origin (Etchevers et al., 2001; Creuzet et al., 2005). Additionally, NCC migration and differentiation have also been visualized using genetically modified mice. Kikuchi et al. (2011) analyzed the migration and differentiation of NCCs using *P0-Cre;EGFP* transgenic mice and showed that EGFP-positive cells were localized in the iris stroma, corneal endothelium and trabecular meshwork. However, cell fate and AES formation might differ between chicken and quail. Gage et al. (2005) reported that the iris stroma originated from the mesoderm and that the corneal endothelium and stroma derived from both the NCCs and mesoderm. In the current study, we could not conclude that aniridia in *Itpr1*$^{\Delta 7bp/\Delta 7bp}$ mice is caused only by the failure of NCC differentiation. However, we demonstrated that p75NTR-positive cells, which are most likely undifferentiated NCCs, remained in the iris and corneal stroma in *Itpr1*$^{\Delta 7bp/\Delta 7bp}$ mice at P21. Our future plan is to cross our mice with NCC-specific or mesoderm-specific marker-expressing mice to determine the fate of periocular mesenchymal cells in AES.

Additionally, in *Itpr1*$^{\Delta 7bp/\Delta 7bp}$ mice, iris smooth muscles derived from the optic cup were lost or sparse and the corneal epithelium originating from the epithelial ectoderm failed to stratify. This suggests that the interaction between the periocular mesenchyme or mesoderm and ectodermal cells is essential for AES formation. Previous experiments have also suggested an interaction between these tissues via growth factors and their downstream signal transduction (Fuhrmann et al., 2000; Kanakubo et al., 2006). However, additional experiments are required to confirm the nature of this interaction.

MATERIALS AND METHODS

Human subjects

This study was approved by the Ethics Committee of Nagasaki University. We received written informed consent from five individuals with GLPS and their healthy parents, and then obtained their blood samples. Genomic DNA extraction was performed in accordance with the conventional proteinase K/phenol and chloroform protocol, followed by dialysis (Green and Sambrook, 2012). Magnetic resonance imaging (MRI) at 1.5 tesla was performed for each patient. Axial and sagittal T1 or T2 weighted images were conducted and representative images were demonstrated.

Exome sequencing

Exome capture was performed using an Agilent SureSelect 55MB Exome Plus kit (Agilent Technologies), in accordance with the manufacturer's protocol. The captured libraries were sequenced using paired-end sequencing on an Illumina HiSeq 2000 system (Illumina). The data were analyzed using our pipeline (Horai et al., 2018). Briefly, read mapping was performed using Novoalign software (Novocraft) and then sorted BAM files were processed by Genome Analysis Tool Kit (GATK) software package (McKenna et al., 2010). Variant calling was performed using HaplotypeCaller in GATK. The mutations identified were confirmed using Sanger sequencing on a 3130xl Genetic Analyzer (Thermo Fisher Scientific).

Generation of *Itpr1-V5* knock-in mice

All animal (*Mus musculus*) experiments in this study were carried out in accordance with Standards Relating to the Care and Keeping and Reducing Pain of Laboratory Animals (Notice of the Japanese Ministry of the Environment No. 88 of 2006) and its latest revision (2013). The animal experimental protocol was approved by the Ethics Committee of Nagasaki University (approval number: 1602151283).

The V5-tag sequence was inserted into the NaeI site adjacent to the stop codon in exon 62 of mouse *Itpr1*. A total of 6.3 kb of the 5′-arm, including V5-tagged exon 62 and 2.4 kb of the 3′-arm, was cloned into the vector containing the floxed phosphoglycerate kinase (*Pgk*) promoter-neomycin resistance gene cassette for positive selection and diphtheria toxin cassette

Development (2021) 148, dev188755. doi:10.1242/dev.188755

for negative selection. The gene-targeting construct was digested with NotI and the linearized product was then electroporated into mouse embryonic stem cells (ESCs) derived from the C57BL/6J strain. Through screening using PCR and Southern hybridization, six homologous recombinants were obtained. ESCs were transferred into mouse ICR blastocysts to establish chimeric mice. Mice that were heterozygous for V5-tagged *Itpr1* were obtained by crossing male chimeras with C57BL/6J female mice. The floxed *Pgk*-neomycin resistance gene cassette was removed by subsequent mating with *CAG-Cre* transgenic mice (Sakai and Miyazaki, 1997). Genotyping PCR was performed using the following primers: 5′-GCAGAGTTCCGAAGCAAGTCAAG-3′ and 5′-TGGGGAAAATGCCAAGTTAAAGG-3′, using KOD FX Neo DNA polymerase (KFX-201; Toyobo).

Determination of the novel TSS of *Itpr1*

Total RNA was extracted from the eyes and brains of P0 mice with a V5-tagged sequence using a NucleoSpin RNA Kit (740955; Macherey-Nagel), followed by DNase I (2270A; Takara) treatment and purification using a NucleoSpin RNA Clean-up kit (740948; Macherey-Nagel). RNA concentration and RNA integrity number were determined using an Agilent RNA 6000 Pico kit (5067-1513; Agilent Technologies) on a 2100 Bioanalyzer. Complementary DNA (cDNA) libraries were prepared using the SMART-Seq v4 Ultra Low Input RNA Kit for Sequencing (Z4888N; Takara). Total RNA (1 µg) was reverse-transcribed using a V5-specific reverse primer with the M13F-20 sequence (5′-CGACGTTGTAAAACGACGGCCAGTNNNNNNGGTGCTGTCCAGGCCCAGCA-3′; N represents any nucleotide for barcoding to distinguish monoclonal products, and the underlined sequence indicates M13-20) or *Itpr1* exon 60-specific primer with the M13-20 sequence (5′-CGACGTTGTAAAACGACGGCCAGTNNNNNNCCACGTAACTCTCAGGCCCGGTGTA-3′) instead of the oligo(dT) primer with the adaptor sequence supplied by the manufacturer. Locked nucleic acid (LNA)-capped cDNA libraries were then amplified using the M13-20 reverse primer and LNA-specific forward primer. Amplified libraries were further amplified with an exon 59-specific reverse primer (5′-CACTCCTCAGGTCAGCAAAGGTGTCA-3′) and a nested LNA forward primer.

Massive parallel sequencing was performed using Illumina HiSeq 2500 (100 bp paired-end reads), while adapter trimming and quality filtration of raw reads were performed using Trim Galore-0.4.4 (https://www.bioinformatics.babraham.ac.uk/projects/trim_galore/). Sequence reads were mapped to mouse GRCm38/mm10 using HISAT-2.1.0 (Pertea et al., 2016) and the sorted BAM files were generated using SAMtools 1.3.1 (Li et al., 2009). BAM files were visualized using Integrative Genomics Viewer (IGV) (Robinson et al., 2011). The sequencing data have been deposited in the DDBJ Sequence Read Archive (DRA) under accession number DRA011309.

Cell culture and transfection

Authentication of human embryonic kidney 293T (HEK293T) cells was conducted by the Japanese Cell Bank of Research Bioresources (JCRB). We also purchased the NIH3T3/Tet-on 3G cell line (631197; Clontech) and O9-1 mouse cranial neural crest cell line (SCC049; Merck Millipore) for this study. All cell lines were cultured at 37°C in an atmosphere containing 95% air and 5% CO_2. HEK293T cells were cultured in high-glucose Dulbecco's modified Eagle's medium supplemented with L-glutamine (DMEM, 044-29765; Fujifilm Wako Pure Chemical Corporation), 10% fetal bovine serum (FBS, 04-001-1A; Biological Industries), and 100 units/ml penicillin/streptomycin (168-23191; Fujifilm Wako Pure Chemical Corporation). The O9-1 cell line was cultured on a Matrigel-coated (354234; Corning)-coated plastic dish filled with complete ESC medium (ES-101-B; Merck Millipore) supplemented with 25 ng/ml FGF-2 (GF003; Merck Millipore). The NIH3T3/Tet-on 3G cell line was cultured in DMEM supplemented with 10% Tet System Approved FBS (Z1107N; Takara).

For HEK293T cells, transfection was performed with polyethylenimine 'Max' (PEI-Max, 24765-1; Polysciences), in which DNA-reagent complexes were prepared using DNA (µg) and PEI-Max reagent (µl) at a 1:2 ratio. For NIH3T3/Tet-on 3G cells, the ScreenFect A Plus reagent (293-73203; Fujifilm Wako Pure Chemical Corporation) was used at the same ratio.

Reporter assay and TF expression vectors

For the reporter assay, chr3:4,854,261-4,854,825 DNA fragments within GRCh37/hg19 were amplified from the human BAC clone RP11-106B10 as a template and cloned into the XhoI site of the pNL1.1[*Nluc*] vector (N1001; Promega). We chose *PAX6*, *PAX6(5a)*, *PITX3*, *MAF*, *FOXC1*, *FOSL2*, *OTX1*, *MSX1* and *PITX2* as candidate TFs. Circular (c)DNAs encoding TFs were amplified via PCR using a human fetal multiple-tissue cDNA panel (Z6748N; Takara) and cloned into the p3×FLAG-CMV-7.1 vector (E7533; Merck Millipore). All plasmids in this study were purified using NucleoBond® Xtra Midi (740410; Macherey-Nagel). In total, 50,000 HEK293T cells were seeded onto 48-well plates and transfected with reporter plasmids (0.25 µg), using the pGL4.54[luc2/TK] vector (E5061; Promega) as an internal control (10 ng), with or without a TF-expressing vector (0.25 µg). After 48 h of incubation, the cells were lysed in 80 µl of 1× Passive Lysis Buffer (E1941; Promega) and clarified using centrifugation at 14,000 rpm (17,800 ***g***) at 4°C for 3 min. The Nano-Glo Dual-Luciferase Reporter Assay System (N1610; Promega) was used for the assay, and the protein concentration was measured using a Protein Assay BCA kit (297-73101; Fujifilm Wako Pure Chemical Corporation). The observed NanoLuc luciferase activity data were normalized to the amount of protein (activity/µg of protein; n=9 for each test).

MAF- and SOX9-binding assays

The 3×FLAG-tagged human MAF or mutant R288P-expressing vector was transfected into HEK293T cells in 10 cm culture dishes. The FLAG-tagged SOX9 or mutant H165Q was also transfected. After 48 h of incubation, nuclear proteins were extracted using the EZSubCell Extract kit (2332337; Atto), and the protein concentration was determined using the BCA assay. FG beads magnetic nanoparticles were purchased from Tamagawa Seiki (TAS8848N1010; Iida). The double-stranded oligonucleotides shown in Fig. S5A for MAF were directly bound to the FG beads, in accordance with the manufacturer's protocol. For SOX9 binding, the double-stranded oligonucleotide 5′-TGTTATTTATGTAAAGAATTGTTTAATCAGCCGTGAATTGGGGACT-3′ was also directly bound (underline indicates the SOX9-binding motif). These FG beads coated with double-stranded oligonucleotides were mixed with 200 µg of nuclear protein at 4°C for 4 h. After washing three times, the FG beads with the nucleotide-protein complex were separated on a SureBeads magnetic rack (1614916; Bio-Rad). Bound proteins were eluted in 1× Laemmli buffer at 100°C for 5 min and then separated using SDS-PAGE, followed by immunoblotting with an anti-FLAG (DDDDK)-tagged mouse monoclonal antibody (1:10,000, M185-3L; MBL).

Chromatin immunoprecipitation assays

HEK293T cells were transfected with the expression vectors of the 3×FLAG-tagged human MAF or 3×FLAG-tagged R288P mutant. After 48 h of incubation, the cells were fixed with formaldehyde at a final concentration of 1% for 10 min. O9-1 cells were fixed under the same conditions. We used a SimpleChIP® Plus Sonication Chromatin IP Kit (56383; Cell Signaling Technology), as per the manufacturer's protocol. For fragmentation, a combination of Covaris S2 system and microtube AFA Fiber Pre-Slit Snap-Cap 6×16 mm (520045; Covaris) was used with a program of 12 min per set, duty 2%, cycle intensity 3 and cycle/burst ratio 200. A total of 2 µg of an anti-FLAG-tag mouse monoclonal antibody (1:250, M185-3L; MBL), an anti-SOX9 rabbit polyclonal antibody (AB5535; Merck Millipore), or normal rabbit IgG1 (2729S; Cell Signaling Technology) was added to each fragmented chromatin solution. To confirm ChIP efficiency, immunoblotting was performed with an anti-FLAG (DDDDK)-tagged mouse monoclonal antibody (1:10,000) and anti-H3 rabbit polyclonal antibody (1:1000, 9715S; Cell Signaling Technology) as an internal control. Quantitative PCR was performed using KOD SYBR qPCR mix (QKD-201; Toyobo) and LightCycler 480 (Roche Diagnostic). The following primers were used to amplify the sequence that included the MAF and SOX9-binding sites: for MAF-binding sites, 5′-AATCTTGCCAGAGTCTGTACGTT-3′ and 5′-ACTTTCATTTGGTGATCTGGATG-3′, and for SOX9 binding sites, 5′-TGCAGTATTGGAGGGTGTTATTTATG-3′, and 5′-TGGGATAGAGAAGGGAGTTTTGTG-3′. PCR conditions were as follows: initial denaturation at 95°C for 2 min; 40 cycles of 95°C for

Development (2021) 148, dev188755. doi:10.1242/dev.188755

15 s, 60°C for 15 s, and 68°C for 20 s; followed by a final extension at 68°C for 5 min [biological replicates (n=3) with three technical replicates].

Determination of the translation start site in the novel transcript of *Itpr1*

Total RNA was isolated from the eyes of *Itpr1*$^{V5/V5}$ mice and reverse-transcribed using a PrimeScript™ II 1st Strand cDNA Synthesis Kit (6210A; Takara). The C-terminal V5-tagged *Itpr1* cDNA fragments were amplified using PCR with PrimeSTAR MAX DNA Polymerase (R045A; Takara) and cloned into the pcDNA3.1(−)-Hyg Mammalian Expression vector (V87520; Thermo Fisher Scientific). Each expression vector was transfected into HEK293T cells and lysed in RIPA buffer [50 mM Tris-HCl (pH 7.6), 150 mM NaCl, 1% Nonidet P-40 (18558-54; Nacalai Tasque), 0.5% sodium deoxycholate and 0.1% SDS] supplemented with a protease inhibitor cocktail (0484-11; Nacalai Tesque), followed by three cycles of sonication for 10 s and centrifugation at 20,000× ***g*** for 10 min. Proteins were resolved using SDS-PAGE and transferred onto polyvinylidene difluoride (PVDF) membranes (033-22453; Fujifilm Wako Pure Chemical Corporation) for immunoblotting. Anti-V5-tagged mouse monoclonal (1:1000, M215-3; MBL) and anti-α-tubulin mouse monoclonal antibodies (1:2000, 017-25031; Fujifilm Wako Pure Chemical Corporation) were used for this assay. Chemiluminescent signals were detected using ImmunoStar Zeta (297-72403; Fujifilm Wako Pure Chemical Corporation) and the ChemiDoc Touch Imaging System (Bio-Rad).

Protein glycosylation analysis

C-terminal V5-tagged mouse *Itpr1* cDNA fragments were cloned into the pcDNA3.1(−)-Hyg mammalian expression vector. GlcNAc-binding sites were predicted using the NetNGlyc 1.0 server (http://www.cbs.dtu.dk/services/NetNGlyc/). Asparagine residues in the two predicted GlcNAc-binding motifs were replaced with lysine by PCR-based mutagenesis. Extracts from transfected cells were treated with EndoH (P0702S; New England BioLabs), according to the manufacturer's protocol, followed by SDS-PAGE and immunoblotting with anti-V5-tagged mouse monoclonal antibody (1:1000). Mouse monoclonal anti-β-actin (1:1000, 010-27841; Fujifilm Wako Pure Chemical Corporation) and mouse monoclonal anti-α-tubulin (1:2000) antibodies were used as internal controls.

Cellular fractionation and immunoblotting

An expression vector encoding the 218-aa isoform of Itpr1 was transfected into the HEK293T cell line. After 48 h of transfection, cellular fractionation was performed using the EZSubCell Extract kit. Immunoblotting was performed using anti-mouse monoclonal V5 (1:1000), anti-mouse monoclonal α-tubulin (1:2000), anti-PDI (C81H6) rabbit monoclonal (1:1000, 3501S; Cell Signaling Technology), and anti-H3 rabbit polyclonal antibodies (1:1000).

Protein extraction from animal tissues and western immunoassays

Ground tissues were lysed in 1× cell lysis buffer (9803; Cell Signaling Technology) supplemented with 1 mM phenylmethylsulfonyl fluoride (8553; Cell Signaling Technology), followed by three cycles of sonication for 10 s each on ice. Protein samples were clarified by centrifugation at 20,000× ***g*** for 15 min at 4°C, and their concentrations were measured using the BCA assay. Total protein samples (2 µg/µl) were separated using a Simple Western WES system (004-600A-N001; ProteinSimple) and a 12-230 kDa WES separation module, with 25 capillary cartridges (SM-W004; ProteinSimple). Immunoassay was performed using anti-V5 (D3H8Q) rabbit monoclonal antibody (1:25, 13202S; Cell Signaling Technology), anti-IP3 receptor 1 rabbit polyclonal antibody (1:25, PA1-901; Thermo Fisher Scientific), anti-SOX9 rabbit polyclonal antibody (1:25, AB5535; Merck Millipore), and anti-GAPDH mouse monoclonal antibody (1:100, 60004-1-Ig; Proteintech).

Generation of *Itpr1*-knockout mice using CRISPR/Cas9

For *in vitro* guide RNA (gRNA) synthesis, DNA oligonucleotide sets were designed to disrupt exons 59 and 62 of mouse *Itpr1*. For exon 59, the following sense and antisense oligonucleotides were used: oligo 1, 5′-agggCGTCCTGAACCTGATTTTCG-3′; antisense oligo 1, 5′-aaacCGAAAATCAGGTTCAGGACG-3′; sense oligo 2, 5′-agggTGATGACCATGAAGAAGAAG-3′; antisense oligo 2, 5′-aaacCTTCTTCTTCATGGTCATCA-3′ (lowercase letters indicate the adaptor sequence for cloning). For exon 62, the sense oligo was 5′-agggGAATGTCAACCCACAGCAGC-3′, and the antisense oligonucleotide was 5′-aaacGCTGCTGTGGGTTGACATTC-3′. Double-stranded DNA oligonucleotides were ligated into T7 gRNA cloning and production vectors (CAS510A-1; System Biosciences), which were then transformed into the ECOS competent *Escherichia coli* DH5α strain (310-06236; Nippon Gene). The vectors were purified using a FastGene Plasmid Mini Kit (FG-90502; Nippon Genetics), and the inserted sequences were confirmed using Sanger sequencing. gRNA templates containing the T7 promoter sequence were amplified using PCR with the attached T7 gRNA PCR primer mix (CAS510A-KIT; System Biosciences). The gRNAs were transcribed *in vitro* using the MEGAscript™ T7 Transcription kit (AMB1333; Thermo Fisher Scientific) with amplicons as a template and purified using a NucleoSpin RNA Clean-up kit (740955; Macherey-Nagel). RNA fragment size and concentration were determined using an Agilent RNA 6000 Nano kit (5067-1511; Agilent Technologies). Transfection-ready hspCas9 SmartNuclease mRNA (CAS500A-1; System Biosciences) and gRNA were microinjected into fertilized C57BL/6J mouse eggs. Genotyping was performed using the DNA extracted from the tail tips of the mice. For exon 59-knockout mice, the genotypes were determined by TA cloning followed by Sanger sequencing. For mice with a deletion of seven base pairs in exon 62, genotypes were determined by direct sequencing using the following primers: 5′-GACGCACAGGAAGTGTCTGA-3′ and 5′-TGGTTCAAGTGCAAATCAGG-3′.

Histological analysis

Isolated murine eyes were fixed in Super Fix (KY-500; Kurabo) and embedded in paraffin. The tissues were sliced to a thickness of 5 µm. H&E staining was performed using Hematoxilin and Eosin Stain Kit (H-3502, Vector Laboratories) according to the manufacturer's instructions. For immunohistochemistry, the slides were unmasked by heating at 98°C for 20 min in citrate buffer (pH 6.0), followed by incubation in 3% hydrogen peroxide for 10 min. The slides were blocked with Protein Block Serum-Free Ready-To-Use (X0909; DAKO) for 1 h at room temperature and then incubated overnight at 4°C with an anti-V5 tag (D3H8Q) rabbit monoclonal antibody (1:200; Cell Signaling Technology) or normal rabbit IgG (1:1000, CTK4721; Wako). After washing three times in 1× PBS for 5 min each, signals were obtained using the SignalStain Boost IHC Detection Reagent (HRP, Rabbit, 8114; Cell Signaling Technology) and SignalStain DAB Substrate Kit (8059; Cell Signaling Technology). The slides were counterstained with hematoxylin, dehydrated and mounted.

For immunofluorescence assays, the slides were incubated overnight at 4°C with the following primary antibodies: anti-V5 tag (D3H8Q) rabbit monoclonal antibody (1:200), anti-Pdpn (clone 8.1.1) Syrian hamster monoclonal antibody (1:1000, MABT1512; Millipore), anti-GRIP1 rabbit polyclonal antibody (1:100, 22398-1-AP; Proteintech), anti-smooth muscle actin (D4K9N) rabbit monoclonal antibody (1:800; 19245; Cell Signaling Technology), anti-p75NTR antibody (1:1600, 8238; Cell Signaling Technology), anti-cleaved caspase-3 (Asp175) (5A1E) rabbit monoclonal antibody (1:400, 9664; Cell Signaling Technology), anti-PAX6 (P3U1) mouse monoclonal antibody (1:200, AB_528427; Developmental Studies Hybridoma Bank, University of Iowa), and anti-β-actin rabbit polyclonal antibody (1:500, GTX109639, GeneTex). After washing, the slides were incubated for 1 h with the following secondary antibodies for the immunofluorescence assay: anti-rabbit IgG (H+L), F(ab)2 fragment Alexa Fluor® 488 conjugate (1:1000, 4412; Cell Signaling Technology), anti-rabbit IgG (H+L), F(ab)2 fragment Alexa Fluor® 555 conjugate (1:1000, 4413S; Cell Signaling Technology), anti-mouse IgG (H+L), F(ab)2 fragment Alexa Fluor® 488 conjugate (1:1000, 4408S; Cell Signaling Technology), anti-mouse IgG (H+L), F(ab)2 fragment Alexa Fluor® 555 conjugate (1:1000, 4409S; Cell Signaling Technology) and anti-Syrian hamster IgG H&L Alexa Fluor® 488 (1:1000, ab180063; Abcam). To reduce autofluorescence, the slides were treated using the TrueVIEW Autofluorescence Quenching kit (SP-8500; Vector Laboratories). Slides were mounted using Vectashield Vibrance Antifade Mounting Medium,

Development (2021) 148, dev188755. doi:10.1242/dev.188755

which included DAPI (H-1800; Vector Laboratories). Immunofluorescence images were obtained using a BZ-X800 microscopy system (Keyence).

Mass spectrometry assay

Total protein (200 µg) extracted from *Itpr1*$^{V5/V5}$ mouse eyes at P0 was immunoprecipitated with the magnetic bead-conjugated anti-V5-tagged mouse monoclonal antibody (M215-11; MBL). Precipitated protein samples were separated on a 10% acrylamide gel and stained using Coomassie Brilliant Blue R 250 (112553; Merck). The protein bands were visualized, clipped from the gel and used for identification of the ITPR1-interacting proteins using MS. The experiment was performed in accordance with the protocol using the murine database instead of the human database (Tanimura et al., 2016).

Immunoprecipitation assay

A vector expressing the C-terminal V5-tagged wild-type or K71Del mutant of the ITPR1 218-aa isoform was transfected into HEK293T cells in 10 cm dishes using the method described above. After 48 h, the cells were lysed in a buffer containing 50 mM Tris-HCl (pH 7.5), 150 mM NaCl, 0.05% NP-40 and 1× protease inhibitor cocktail, followed by sonication and centrifugation (17,800 ***g***). A total of 200 µg of supernatant was incubated with the magnetic bead-conjugated anti-V5-tagged mouse monoclonal antibody (1:100) overnight. The next morning, protein-bound beads were washed three times with 1× PBS and eluted in 1× SDS sample buffer. The eluted proteins were separated on 4-20% mini-protean TGX Stain-Free gel (4568093; Bio-Rad). Immunoblotting was performed using mouse monoclonal anti-β-actin (1:1000), rabbit polyclonal anti-myosin IIa (1:1000, 3403; Cell Signaling Technology) and anti-vinculin (2B5A7) mouse monoclonal antibody (1:5000, 66305-1-Ig, Proteintech).

Doxycycline-inducible expression of ITPR1 218-aa isoform in NIH3T3/Tet-on 3G cells

The *Xho*I fragment of the hygromycin resistance cassette from the pTRE2hyg vector (Z1014N; Clontech) was cloned into the site of the pTRE-Tight vector (Z1059N; Clontech). cDNA encoding the 218-aa isoform of ITPR1 with a V5-tagged sequence was then cloned into the modified vector. NIH3T3/Tet-on 3G cells were seeded at a density of 200,000 per well in a six-well plate and transfected with 2 µg of the doxycycline-inducible expression vector. After 2 days, cells were split into four 10 cm dishes and selected using 200 µg/ml Hygromycin B Gold (ant-hg-1; InvivoGen) for 2 weeks. Single colonies were transferred into single wells of 24-well plates. Cells were treated with doxycycline (Z1311; Takara) at a final concentration of 1 µg/ml for 24-48 h to induce expression.

Immunofluorescence assays were performed with anti-V5 tag (D3H8Q) rabbit monoclonal antibody (1:1000), anti-PDI (C81H6) rabbit monoclonal antibody (1:100) and anti-Lamin A/C (4C11) mouse monoclonal antibody (1:200, 4777; Cell Signaling Technology) in accordance with the protocol supplied by Cell Signaling Technology. Actin staining was performed using Acti-stain™ 488 phalloidin (PHDG1-A; Cytoskeleton), following the manufacturer's protocol. Mounting was carried out with mounting medium for fluorescence, which included DAPI. Cell migration assays were performed in accordance with the procedure reported by Tanimura et al. (2016). Immunoblotting and quantification were performed using Simple Western WES system with rabbit monoclonal anti-YAP (1:50) and mouse monoclonal Lamin A/C (1:50) antibodies

Measurement of vinculin and YAP signal

Immunofluorescence assays were performed in accordance with the protocol supplied by Cell Signaling Technology. The primary antibodies included an anti-V5 mouse monoclonal antibody (1:1000), an anti-vinculin rabbit polyclonal antibody (1:400, Ab73412; Abcam) and anti-YAP (D8H1X) XP rabbit monoclonal antibody (1:100, 14074; Cell Signaling Technology). The secondary antibodies used were anti-rabbit IgG (H+L), F(ab)2 fragment Alexa Fluor® 488 conjugate and anti-mouse IgG (H+L), F(ab)2 fragment Alexa Fluor® 555 conjugate. Actin staining was performed using Acti-stain™ 488 phalloidin (PHDG1-A; Cytoskeleton), following the manufacturer's protocol. Mounting was carried out with mounting medium for fluorescence, which included DAPI.

Quantification of protein expression using fluorescence intensity as an index was performed as previously described (de Kerckhove et al., 2018). Briefly, at least three randomly selected fields of view per group (magnification, ×20) were scanned using a confocal laser scanning unit microscope ($C2_+$ system, Nikon) equipped with Plan Apo VC20X (0.75 NA) and NIS-Elements C software version 4.13 (Nikon). Vinculin- and YAP-positive areas were delineated using the freehand drawing tool and the fluorescence intensity was measured using AR software version 4.0 (Nikon).

Statistical methods

Post hoc Dunnett's test was performed with ANOVA using the SAS software package (version 9.3; SAS Institute). Data are expressed as mean±s.e.m. Differences were significant at $P<0.05$. Student's *t*-test was performed with GraphPad (GraphPad Software).

Acknowledgements

We thank all the families for their participation in this study. We also thank C. Koga and T. Motoyama for their technical assistance. Finally, we are grateful to Edanz (https://en-author-services.edanz.com/ac) for editing the English text of a draft of this manuscript.

Competing interests

The authors declare no competing or financial interests.

Author contributions

Conceptualization: A.K.; Methodology: A.K., R.M.; Software: H.M.; Validation: A.K.; Formal analysis: A.K., K.O.; Investigation: A.K., K.O., S.T., K.M., T.K., Y.N., N.A., H.S., K.H., K.T., N.I., H.M., R.M., M.N.; Resources: A.K., Y.N., N.A., S.H., K.H., K.T., N.I.; Writing - original draft: A.K.; Writing - review & editing: S.S., K.Y.; Visualization: A.K.; Supervision: K.Y.; Project administration: A.K., S.S., K.Y.; Funding acquisition: A.K., S.S.

Funding

This study was supported by Japan Society for the Promotion of Science KAKENHI grants (19K09993 to A.K. and JP26670507 to S.S.).

Data availability

RNA-seq data have been deposited in the DDBJ Sequence Read Archive (DRA) under accession number DRA011309.

Peer review history

The peer review history is available online at https://journals.biologists.com/dev/article-lookup/doi/10.1242/dev.188755

References

Adler, R. and Canto-Soler, M. V. (2007). Molecular mechanisms of optic vesicle development: complexities, ambiguities and controversies. *Dev. Biol.* **305**, 1-13. doi:10.1016/j.ydbio.2007.01.045

Altschul, S. F., Gish, W., Miller, W., Myers, E. W. and Lipman, D. J. (1990). Basic local alignment search tool. *J. Mol. Biol.* **215**, 403-410. doi:10.1016/S0022-2836(05)80360-2

Anand, D., Agrawal, S. A., Slavotinek, A. and Lachke, S. A. (2018). Mutation update of transcription factor genes FOXE3, HSF4, MAF, and PITX3 causing cataracts and other developmental ocular defects. *Hum. Mutat.* **39**, 471-494. doi:10.1002/humu.23395

Axton, R., Hanson, I., Danes, S., Sellar, G., van Heyningen, V. and Prosser, J. (1997). The incidence of PAX6 mutation in patients with simple aniridia: an evaluation of mutation detection in 12 cases. *J. Med. Genet.* **34**, 279-286. doi:10.1136/jmg.34.4.279

Birke, K., Lütjen-Drecoll, E., Kerjaschki, D. and Birke, M. T. (2010). Expression of podoplanin and other lymphatic markers in the human anterior eye segment. *Invest. Ophthalmol. Vis. Sci.* **51**, 344-354. doi:10.1167/iovs.08-3307

Carvalho, D. R., Medeiros, J. E. G., Ribeiro, D. S. M., Martins, B. J. A. F. and Sorbeira, N. L. M. (2018). Additional features of Gillespie syndrome in two Brazilian siblings with a novel *ITPR1* homozygous pathogenic variant. *Eur. J. Med. Genet.* **61**, 134-138. doi:10.1016/j.ejmg.2017.11.005

Chen, B., Qi, C.-Y., Chen, L., Dai, M.-J., Miao, Y.-Y., Chen, R., Wei, W.-E., Yang, S., Wang, H.-L., Duan, X.-G. et al. (2020). A C1976Y missense mutation in the mouse of *Ip3r1* gene leads to short-term mydriasis and unfolded protein response in the iris constrictor muscles. *Exp. Anim.* **69**, 45-53. doi:10.1538/expanim.19-0007

Creuzet, S., Vincent, C. and Couly, G. (2005). Neural crest derivatives in ocular and periocular structures. *Int. J. Dev. Biol.* **49**, 161-171. doi:10.1387/ijdb.041937sc

Cvekl, A. and Tamm, E. R. (2004). Anterior eye development and ocular mesenchyme: new insights from mouse models and human diseases. *BioEssays* **26**, 374-386. doi:10.1002/bies.20009
Davis-Silberman, N. and Ashery-Padan, R. (2008). Iris development in vertebrates; genetic and molecular considerations. *Brain Res.* **1192**, 17-28. doi:10.1016/j.brainres.2007.03.043
de Kerckhove, M., Tanaka, K., Umehara, T., Okamoto, M., Kanematsu, S., Hayashi, H., Yano, H., Nishiura, S., Tooyama, S., Matsubayashi, Y. et al. (2018). Targeting *miR*-223 in neutrophils enhances the clearance of *Staphylococcus aureus* in infected wounds. *EMBO Mol. Med.* **10**, e9024. doi:10.15252/emmm.201809024
Dentici, M. L., Barresi, S., Nardella, M., Bellacchio, E., Alfieri, P., Bruselles, A., Pantaleoni, F., Danieli, A., Iarossi, G., Cappa, M. et al. (2017). Identification of novel and hotspot mutations in the channel domain of ITPR1 in two patients with Gillespie syndrome. *Gene* **628**, 141-145. doi:10.1016/j.gene.2017.07.017
Dupont, S., Morsut, L., Aragona, M., Enzo, E., Giulitti, S., Cordenonsi, M., Zanconato, F., Le Digabel, J., Forcato, M., Bicciato, S. et al. (2011). Role of YAP/TAZ in mechanotransduction. *Nature* **474**, 179-183. doi:10.1038/nature10137
Elosegui-Artola, A., Andreu, I., Beedle, A. E. M., Lezamiz, A., Uroz, M., Kosmalska, A. J., Oria, R., Kechagia, J. Z., Rico-Lastres, P., Le Roux, A.-L. et al. (2017). Force triggers YAP nuclear entry by regulating transport across nuclear pores. *Cell* **171**, 1397-1410. doi:10.1016/j.cell.2017.10.008
Etchevers, H. C., Vincent, C., Le Douarin, N. M. and Couly, G. F. (2001). The cephalic neural crest provides pericytes and smooth muscle cells to all blood vessels of the face and forebrain. *Development* **128**, 1059-1068. doi:10.1242/dev.128.7.1059
Eychène, A., Rocques, N. and Pouponnot, C. (2008). A new MAFia in cancer. *Nat. Rev. Cancer* **8**, 683-693. doi:10.1038/nrc2460
Fan, G., Baker, M. L., Wang, Z., Baker, M., Sinyagovskly, P. A., Chiu, W., Ludtke, S. J. and Serysheva, I. I. (2015). Gating machinery of InsP3R channels revealed by electron cryomicroscopy. *Nature* **527**, 336-341. doi:10.1038/nature15249
Ferrari, P. A. and Koch, W. E. (1984). Development of the iris in the chicken embryo. I. A study of growth and histodifferentiation utilizing immunocytochemistry for muscle differentiation. *J. Embryol. Exp. Morph.* **81**, 153-167. doi:10.1242/dev.81.1.153
Fuhrmann, S., Levine, E. M. and Reh, T. A. (2000). Extraocular mesenchyme patterns the optic vesicle during early eye development in the embryonic chick. *Development* **127**, 4599-4609. doi:10.1242/dev.127.21.4599
Gage, P. J., Rhoades, W., Prucka, S. K. and Hjalt, T. (2005). Fate maps of neural crest and mesoderm in the mammalian eye. *Invest. Ophthalmol. Vis. Sci.* **46**, 4200-4208. doi:10.1167/iovs.05-0691
Gerber, S., Alzayady, K. J., Burglen, L., Brémond-Gignac, D., Marchesin, V., Roche, O., Rio, M., Funalot, B., Calman, R., Durr, A. et al. (2016). Recessive and dominant de novo ITPR1 mutations cause Gillespie syndrome. *Am. J. Hum. Genet.* **98**, 971-980. doi:10.1016/j.ajhg.2016.03.004
Gillespie, F. D. (1965). Aniridia, cerebellar ataxia, and oligophrenia in siblings. *Arch. Ophthal.* **73**, 338-341. doi:10.1001/archopht.1965.00970030340008
Green, M. R. and Sambrook, J. (2012) *Molecular Cloning: A Laboratory Manual (Fourth Edition)*, pp. 47-53. Cold Spring Harbor, New York: Cold Spring Harbor Press.
Hägglund, A.-C., Jones, I. and Carlsson, L. (2017). A novel mouse model of anterior segment dysgenesis (ASD): conditional deletion of *Tsc1* disrupts ciliary body and iris development. *Dis. Model. Mech.* **10**, 245-257. doi:10.1242/dmm.028605
Heavner, W. and Pevny, L. (2012). Eye development and retinogenesis. *Cold Spring Harb. Perspect. Biol.* **4**, a008391. doi:10.1101/cshperspect.a008391
Horai, M., Mishima, H., Hayashida, C., Kinoshita, A., Nakane, Y., Matsuo, T., Tsuruda, K., Yanagihara, K., Sato, S., Imanishi, D. et al. (2018). Detection of de novo single nucleotide variants in offspring of atomic-bomb survivors close to the hypocenter by whole-genome sequencing. *J. Hum. Genet.* **63**, 357-363. doi:10.1038/s10038-017-0392-9
Huang, L., Chardon, J. W., Carter, M. T., Friend, K. L., Dudding, T. E., Schwartzentruber, J., Zou, R., Schofield, P. W., Douglas, S., Bulman, D. E. et al. (2012). Missense mutations in ITPR1 cause autosomal dominant congenital nonprogressive spinocerebellar ataxia. *Orphanet J. Rare Dis.* **7**, 67. doi:10.1186/1750-1172-7-67
Iwaki, A., Kawano, Y., Miura, S., Shibata, H., Matsuse, D., Li, W., Furuya, H., Ohyagi, Y., Taniwaki, T., Kira, J. et al. (2008). Heterozygous deletion of ITPR1, but not SUMF1, in spinocerebellar ataxia type 16. *J. Med. Genet.* **45**, 32-35. doi:10.1136/jmg.2007.053942
Jafari, R. and Amiri, A. A. (2015). A clinical and genetic review of aniridia. *J. Pediat. Rev.* **3**, e241. doi:10.17795/jpr-241
Johnston, M. C., Noden, D. M., Hazelton, R. D., Coulombre, J. L. and Coulombre, A. J. (1979). Origins of avian ocular and periocular tissues. *Exp. Eye Res.* **29**, 27-43. doi:10.1016/0014-4835(79)90164-7
Kanakubo, S., Nomura, T., Yamamura, K.-I., Miyazaki, J.-I., Tamai, M. and Osumi, N. (2006). Abnormal migration and distribution of neural crest cells in Pax6 heterozygous mutant eye, a model for human eye diseases. *Genes Cells* **11**, 919-933. doi:10.1111/j.1365-2443.2006.00992.x
Kaser-Eichberger, A., Schrödl, F., Trost, A., Strohmaier, C., Bogner, B., Runge, C., Motloch, K., Bruckner, D., Motloch, K., Bruckner, D. et al. (2015). Topography of lymphatic markers in human iris and ciliary body. *Invest. Ophthalmol. Vis. Sci.* **56**, 4943-4953. doi:10.1167/iovs.15-16573
Kikuchi, M., Hayashi, R., Kanakubo, S., Ogasawara, A., Yamato, M., Osumi, N. and Nishida, K. (2011). Neural crest-derived multipotent cells in the adult mouse iris stroma. *Genes Cells* **16**, 273-281. doi:10.1111/j.1365-2443.2011.01485.x
Kim, J. I., Li, T., Ho, I.-C., Grusby, M. J. and Glimpher, L. H. (1999). Requirement for the c-Maf transcription factor in crystallin gene regulation and lens development. *Proc. Natl. Acad. Sci. USA* **96**, 3781-3785. doi:10.1073/pnas.96.7.3781
Koller, A., Schlossmann, J., Ashman, K., Uttenweiler-Joseph, S., Ruth, P. and Hofmann, F. (2003). Association of phospholamban with a cGMP kinase signaling complex. *Biochem. Biophys. Res. Commun.* **300**, 155-160. doi:10.1016/S0006-291X(02)02799-7
Li, H., Handsaker, B., Wysoker, A., Fennell, T., Ruan, J., Homer, N., Marth, G., Abecasis, G., Durbin, R. and **1000 Genome Project Data Processing Subgroup**. (2009). The Sequence Alignment/Map format and SAMtools. *Bioinformatics* **25**, 2078-2079. doi:10.1093/bioinformatics/btp352
McKenna, A., Hanna, M., Banks, E., Sivachenko, A., Cibulskis, K., Kernytsky, A., Garimella, K., Altshuler, D., Gabriel, S., Daly, M. et al. (2010). The Genome Analysis Toolkit: a MapReduce framework for analyzing next-generation DNA sequencing data. *Genome Res.* **20**, 1297-1303. doi:10.1101/gr.107524.110
MacLean, H. E., Kim, J. I., Glimcher, M. J., Wang, J., Kronenberg, H. M. and Glimcher, L. H. (2003). Absence of transcription factor c-Maf causes abnormal terminal differentiation of hypertrophic chondrocytes during endochondral bone development. *Dev. Biol.* **262**, 51-63. doi:10.1016/S0012-1606(03)00324-5
Maeda, N., Niinobe, M. and Mikoshiba, K. (1990). A cerebellar Purkinje cell marker P400 protein is an inositol 1,4,5-trisphosphate (InsP3) receptor protein. Purification and characterization of InsP3 receptor complex. *EMBO J.* **9**, 61-67. doi:10.1002/j.1460-2075.1990.tb08080.x
Mann, I. C. (1925). The development of the human iris. *Br. J. Ophthalmol.* **9**, 495-512. doi:10.1136/bjo.9.10.495
Matsumoto, M., Nakagawa, T., Inoue, T., Nagata, E., Tanaka, K., Takano, H., Minowa, O., Kuno, J., Sakakibara, S., Yamada, M. et al. (1996). Ataxia and epileptic seizures in mice lacking type 1 inositol 1,4,5-triphosphate receptor. *Nature* **379**, 168-171. doi:10.1038/379168a0
Mayor, C., Brudno, M., Schwartz, J. R., Poliakov, A., Rubin, E. M., Frazer, K. A., Pachter, L. S. and Dubchak, I. (2000). VISTA: visualizing global DNA sequence alignments of arbitrary length. *Bioinformatics* **16**, 1046-1047. doi:10.1093/bioinformatics/16.11.1046
McEntagart, M., Williamson, K. A., Rainger, J. K., Wheeler, A., Seawright, A., De Baere, E., Verdin, H., Bergendahl, T., Quigley, A., Rainger, J. et al. (2016). A restricted repertoire of de novo mutations in ITPR1 cause Gillespie syndrome with evidence for dominant-negative effect. *Am. J. Hum. Genet.* **98**, 981-992. doi:10.1016/j.ajhg.2016.03.018
Paganini, L., Pesenti, C., Milani, D., Fontana, L., Motta, S., Sirchia, S. M., Scuvera, G., Marchisio, P., Esposito, S., Cinnante, C. M. et al. (2018). A novel splice site variant in ITPR1 gene underlying recessive Gillespie syndrome. *Am. J. Med. Genet. A* **176**, 1427-1431. doi:10.1002/ajmg.a.38704
Pan, W., Kremer, K. L., Kaidonis, X., Ludlow, V. E., Rogers, M. L., Xie, J., Proud, C. G. and Koblar, S. A. (2016). Characterization of p75 neurotrophin receptor expression in human dental pulp stem cells. *Int. J. Dev. Neurosci.* **53**, 90-98. doi:10.1016/j.ijdevneu.2016.07.007
Pertea, M., Kim, D., Pertea, G. M., Leek, J. T. and Salzberg, S. L. (2016). Transcript-level expression analysis of RNA-seq experiments with HISAT, StringTie and Ballgown. *Nat. Protoc.* **11**, 1650-1667. doi:10.1038/nprot.2016.095
Rivière, J.-B., Van Bon, B. W. M., Hoischen, A., Kholmanskikh, S. S., O'Roak, B. J., Gilissen, C., Gijsen, S., Sullivan, C. T., Christian, S. L., Abdul-Rahman, O. A. et al. (2012). De novo mutations in the actin genes *ACTB* and *ACTG1* cause Baraitser-Winter syndrome. *Nat. Genet.* **44**, 440-444. doi:10.1038/ng.1091
Robinson, J. T., Thorvaldsdóttir, H., Winckler, W., Guttman, M., Lander, E. S., Getz, G. and Mesirov, J. P. (2011). Integrative genomics viewer. *Nat. Biotechnol.* **29**, 24-26. doi:10.1038/nbt.1754
Sakai, K. and Miyazaki, J.-I. (1997). A transgenic mouse line that retains cre recombinase activity in mature oocytes irrespective of the cre transgene transmission. *Biochem. Biophys. Res. Commun.* **237**, 318-324. doi:10.1006/bbrc.1997.7111
Samuels, I. S., Bell, B. A., Sturgill-Short, G., Ebke, L. A., Rayborn, M., Shi, L., Nishina, P. M. and Peachey, N. S. (2013). Myosin 6 is required for iris development and normal function of the outer retina. *Invest. Ophthalmol. Vis. Sci.* **54**, 7223-7233. doi:10.1167/iovs.13-12887
Sandelin, A., Alkema, W., Engström, P., Wasserman, W. W. and Lenhard, B. (2004). JASPAR: an open-access database for eukaryotic transcription factor binding profiles. *Nucleic Acids Res.*. **32**, D91-D94. doi:10.1093/nar/gkh012
Sasaki, M., Ohba, C., Iai, M., Hirabayashi, S., Osaka, H., Hiraide, T., Saitsu, H. and Matsumoto, N. (2015). Sporadic infantile-onset spinocerebellar ataxia caused by missense mutations of the inositol 1,4,5-triphosphate receptor type 1 gene. *J. Neurol.* **262**, 1278-1284. doi:10.1007/s00415-015-7705-8

Schlossmann, J., Ammendola, A., Ashman, K., Zong, X., Huber, A., Neubauer, G., Wang, G.-X., Allescher, H. D., Korth, M., Wilm, M. et al. (2000). Regulation of intracellular calcium by a signaling complex of IRAG, IP_3 receptor and cGMP kinase Iβ. *Nature.* **404**, 197-201. doi:10.1038/35004606

Shaw, M. W., Falls, H. F. and Neel, J. V. (1960). Congenital aniridia. *Am. J. Hum. Genet.* **12**, 389-415.

Suzuki, A., Kawano, S., Mitsuyama, T., Suyama, M., Kanai, Y., Shirahige, K., Sasaki, H., Tokunaga, K., Tsuchihara, K., Sugano, S. et al. (2018). DBTSS/DBKERO for integrated analysis of transcriptional regulation. *Nucleic Acids Res.* **46**, D229-D238. doi:10.1093/nar/gkx1001

Synofzik, M., Beetz, C., Bauer, C., Bonin, M., Sanchez-Ferrero, E., Schmitz-Hübsch, T., Wüllner, U., Nägele, T., Riess, O., Schöls, L. et al. (2011). Spinocerebellar ataxia type 15: diagnostic assessment, frequency, and phenotypic features. *J. Med. Genet.* **48**, 407-412. doi:10.1136/jmg.2010.087023

Tanimura, S., Hashizume, J., Arichika, N., Watanabe, K., Ohyama, K., Takeda, K. and Kohno, M. (2016). ERK signaling promotes cell motility by inducing the localization of myosin 1E to lamellipodial tips. *J. Cell Biol.* **214**, 475-489. doi:10.1083/jcb.201503123

Trainor, P. A. and Tam, P. P. (1995). Cranial paraxial mesoderm and neural crest cells of the mouse embryo: co-distribution in the craniofacial mesenchyme but distinct segregation in branchial arches. *Development* **121**, 2569-2582. doi:10.1242/dev.121.8.2569

Uhlén, M., Fagerberg, L., Hallström, B. M., Lindskog, C., Oksvold, P., Mardinoglu, A., Sivertsson, Å., Kampf, C., Sjöstedt, E., Asplund, A. et al. (2015). Tissue-based map of the human proteome. *Science* **347**, 1260419. doi:10.1126/science.1260419

Wang, J., Xiao, Y., Hsu, C.-W., Martinez-Traverso, I. M., Zhang, M., Bai, Y., Ishii, M., Maxson, R. E., Olson, E. N., Dickinson, M. E. et al. (2016). Yap and Taz play a crucial role in neural crest-derived craniofacial development. *Development* **143**, 504-515. doi:10.1242/dev.126920

Wicki, A., Lehembre, F., Wick, N., Hantusch, B., Kerjaschki, D. and Christofori, G. (2006). Tumor invasion in the absence of epithelial-mesenchymal transition: Podoplanin-mediated remodeling of the actin cytoskeleton. *Cancer Cell* **9**, 261-272. doi:10.1016/j.ccr.2006.03.010

Xie, Q. and Cvekl, A. (2011). The orchestration of mammalian tissue morphogenesis through a series of coherent feed-forward loops. *J. Biol. Chem.* **286**, 43259-43271. doi:10.1074/jbc.M111.264580

Yates, A. D., Achuthan, P., Akanni, W., Allen, J., Allen, J., Alvarez-Jarreta, J., Amode, M. R., Armean, I. M. Azov, A. G. Bennett, R. et al. (2019). Ensembl 2020. *Nucleic Acids Res.* **48**, D682-D688. doi:10.1093/nar/gkz966

Yoshihara, M., Ohmiya, H., Hara, S., Kawasaki, S., FANTOM consortium, Hayashizaki, Y., Itoh, M., Kawaji, H., Tsujikawa, M. and Nishida, K. (2015). Discovery of molecular markers to discriminate corneal endothelial cells in the human body. *PLoS One* **10**, e0117581. doi:10.1371/journal.pone.0117581